Lb. 1406

ANL-77-17

ANL-77-17

·82
9-13-77

HIGH-PERFORMANCE BATTERIES FOR STATIONARY ENERGY STORAGE AND ELECTRIC-VEHICLE PROPULSION

Progress Report for the Period October–December 1976

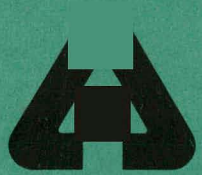

U of C-AUA-USERDA

ARGONNE NATIONAL LABORATORY, ARGONNE, ILLINOIS

Prepared for the U. S. ENERGY RESEARCH AND DEVELOPMENT ADMINISTRATION under Contract W-31-109-Eng-38

DISCLAIMER

Printed in the United States of America
Available from
National Technical Information Service
U. S. Department of Commerce
5285 Port Royal Road
Springfield, Virginia 22161
Price: Printed Copy ~~$5.00~~ $5.25; Microfiche $3.00

Distribution Category:
Energy Storage—Electrochemical
(UC-94c)

ANL-77-17

ARGONNE NATIONAL LABORATORY
9700 South Cass Avenue
Argonne, Illinois 60439

HIGH-PERFORMANCE BATTERIES FOR STATIONARY ENERGY STORAGE AND ELECTRIC-VEHICLE PROPULSION

Progress Report for the Period
October—December 1976

P. A. Nelson	Director, Energy Storage
N. P. Yao	Associate Director, Energy Storage
R. K. Steunenberg	Manager, Lithium/Metal Sulfide Battery Program
A. A. Chilenskas	Manager, Battery Commercialization
E. C. Gay	Section Manager, Battery Engineering
J. E. Battles	Group Leader, Materials Development
F. Hornstra	Group Leader, Battery Charging Systems
W. E. Miller	Group Leader, Industrial Cell and Battery Testing
M. F. Roche	Group Leader, Cell Chemistry
H. Shimotake	Group Leader, Cell Development and Engineering

April 1977

Previous Reports in this Series

ANL-76-9	July—December 1975
ANL-76-35	January—March 1976
ANL-76-81	April—June 1976
ANL-76-98	July—September 1976

PREFACE

The program on high-temperature secondary batteries at Argonne National Laboratory is carried out principally in the Chemical Engineering Division, with assistance on specific problems being given by the Materials Science Division and, from time to time, by other Argonne divisions. The individual efforts of many scientists, engineers, and technicians are essential to the success of the program, and recognition of these efforts is reflected by the individual contributions cited throughout the report.

TABLE OF CONTENTS

TABLE OF CONTENTS (cont'd)

LIST OF FIGURES

LIST OF TABLES

HIGH-PERFORMANCE BATTERIES FOR STATIONARY ENERGY STORAGE AND ELECTRIC-VEHICLE PROPULSION

Progress Report for the Period
October—December 1976

ABSTRACT

This report describes the research, development, and management activities of the program at Argonne National Laboratory (ANL) on lithium-aluminum/metal sulfide batteries during the period October-December 1976. These batteries are being developed for electric vehicle propulsion and for stationary energy storage applications. The present battery cells, which operate at 400-450°C, are of a vertically oriented, prismatic design with a central positive electrode of FeS or FeS_2, two facing negative electrodes of lithium-aluminum alloy, and an electrolyte of molten LiCl-KCl.

A major objective of this program is to transfer the technology to industry as it is developed, with the ultimate goal of a competitive, self-sustaining industry for the commercial production of lithium-aluminum/metal sulfide batteries. Technology transfer is being implemented by several means, including the assignment of industrial participants to ANL laboratories for various periods of time and the subcontracting of development and fabrication work on cells, cell components and battery testing equipment to industrial firms.

Testing and evaluation of industrially fabricated cells is continuing. During this period, Li-Al/FeS and Li-Al/FeS_2 cells from Eagle-Picher Industries have been tested, and tests of Li-Al/FeS cells from Gould Inc. have been initiated. The cells are tested individually and in parallel and series battery configurations. These tests provide information on the effects of cell design modifications and alternative materials. Improved electrode and cell designs are being developed and tested at ANL, and the more promising designs are incorporated in the industrially fabricated cells. Among the concepts receiving major attention are carbon-bonded positive electrodes, scaled-up stationary energy storage cell designs, additives to extend electrode lifetime, and alternative electrode separators.

The materials development efforts include the development of a new lightweight electrical feedthrough; investigations of new separator materials (*e.g.*, Y_2O_3 powder, Y_2O_3 felt, and porous, rigid ceramics); corrosion tests of materials for cell components; and postoperative examinations of cells. The cell chemistry studies were directed to discharge mechanisms of FeS electrodes, emf measurements of the LiAl/FeS_2 couple at various states of discharge, and studies of other transition-metal sulfides as positive-electrode materials. The advanced battery effort mainly concerned the use of calcium alloys for the negative electrode and transition metal sulfides or oxides for the positive electrode.

SUMMARY

Commercial Development

The objective of the commercial development effort is to assist in the establishment of a competitive, self-sustaining industry capable of producing a supply of lithium/metal sulfide batteries that will meet national needs. A commercial development plan that consists of a market study, an analysis of battery cost as a function of production rate, a manufacturing plan, a financial plan, and an analysis of competing technologies has been initiated.

Calculations were made that related the efficiency of battery for two types of automobiles (compact and family) to the miles driven per year and the amount of heat loss through the battery insulation during the year. The results led to the following conclusions: (1) the energy efficiencies of both batteries are very sensitive to the miles driven per year and the battery heat loss; (2) the cost of maintaining the battery temperature can be reduced to zero for automobiles that are driven ∿6000-10,000 km per year if the batteries are well insulated; and (3) heat loss rates of 75-100 W for a 30 kW-hr compact car battery and 150-200 W for a 50 kW-hr family car battery are acceptable for normal driving patterns. In addition, heat-loss calculations have indicated that a 1-cm-thick vacuum-foil insulated jacket is likely to meet the requirements for an electric-vehicle battery. A vacuum-foil insulated jacket for use in a six-cell battery test is being prepared by Linde (a division of Union Carbide Corp.).

A conceptual design and cost study of a 5 MW-hr truckable module that is suitable for testing in the BEST (Battery Energy Storage Test) Facility has been completed. The lithium/iron sulfide battery module is expected to be ready for testing in the BEST Facility in 1981 or 1982.

The commercialization plan for Li-Al/metal sulfide batteries includes contractual arrangements with industrial firms to develop and fabricate cells, cell components, battery components, and battery testing equipment. Gould Inc. has completed the fabrication of six uncharged Li-Al/FeS cells with 13 x 18 cm (5 x 7 in.) hot-pressed electrodes. The present effort at Eagle-Picher Industries, Inc. is directed toward the production of 58 Li-Al/FeS cells with 13 x 13 cm (5 x 5 in.) cold-pressed, uncharged FeS electrodes. These Eagle-Picher cells incorporate several design variations, such as the ratio of positive and negative electrode capacities, size of the positive current lead, and the type of electrode separator. Eagle-Picher is also involved in a cooperative effort with ANL in a design study of a housing for a 30-kW-hr electric vehicle battery. The Catalyst Research Corp. is continuing to develop simplified procedures for the fabrication of cells. The Carborundum Corp. is producing BN fiber for near-term use in cell separators and has developed prototype paper separators of BN fibers bonded with BN. A process for the production of Li_2S from Li_2CO_3 and H_2S has been developed by Eagle-Picher for use in uncharged cells. Various other contracts with industrial firms involve the development of alternative separators such as BN and Y_2O_3 felts, and the development of electrical feedthroughs.

A contract with International Harvester on the development of a computer-controlled simulator for electric-vehicle load profiles has been completed.

A computer program has also been developed to calculate the effects of variations in the control and power-train elements on the range and performance of electric vehicles. Although the computer program has not yet been fully verified, simulated runs for a lead-acid battery vehicle have given results that are in good agreement with published data of road tests for similar batteries.

Industrial Cell and Battery Testing

Testing of Li-Al/FeS_2 cells fabricated by Eagle-Picher has continued at ANL. The electrodes were made by cold-pressing the active powder into honeycomb current collector structures. The Eagle-Picher cells are of two types and differ from each other principally in electrode thickness. In the Type A (thin) cells, the negative electrode thicknesses and the positive electrode half-thicknesses are both 0.35 cm. In the Type B (thick) cells, the negative electrodes are 0.7 cm thick and the half-thicknesses of the positive electrode are 0.6 cm.

Three Type B Li-Al/FeS_2 cells (EP-2B4, -2B5, and 2B7) were deep cycled at constant current charge and discharge to test the effects of changing the charge cutoff voltage. The results showed that increasing the charge cutoff voltage from 2.0 to 2.2 V increased the cell capacity from 80 to 114 A-hr. A reduction of the charge cutoff voltage from 2.2 to 2.0 V had no significant effect on cell lifetime. Testing of Cell EP-2B4 was terminated after 1700 hr and 130 cycles because of declining capacity, and testing of Cell EP-2B5 was terminated after 2175 hr and 127 cycles because of decreasing coulombic efficiency. Cell EP-2B7 continues to operate well after more than 1850 hr and 350 cycles, with a specific energy of 40 W-hr/kg at the 2-hr rate.

The Type A Li-Al/FeS_2 cells tend to have a higher specific power but lower specific energy than the Type B cells. Typical performance for the Type A cells was reflected in the performance of EP-2A5. This cell had an initial specific energy of 66 W-hr/kg (4.1-hr rate), which declined to 42 W-hr/kg after 200 deep cycles. The Type A cells have not shown the dependence of capacity on charge cutoff voltage as was observed with the Type B cells.

Tests have been initiated on the first Li-Al/FeS cells from Eagle-Picher which are deviations from the baseline Type B design. The first design variation to be tested is the use of separators using Y_2O_3 felt, rather than BN fabric. Failures of two of these cells and one ANL cell using the Y_2O_3-felt separator after 400 to 500 hr indicated that this type of separator is not compatible with the current cell designs and fabrication procedures.

Four Li-Al/FeS cells with 13 x 18 cm (5 x 7 in.) hot-pressed, uncharged electrodes have been received from Gould. Tests of these cells have been started.

A cell design model has been developed to evaluate the effects of design changes on the specific energy and power of the cells. The modeling studies have shown that the ratio of active material to cell weight in current cell designs should be increased, but that this can be done only by shaving the weights of several components. The studies also indicate that greater utilization of the active material would be highly beneficial.

Testing of cells in a series arrangement was conducted to study the interactions of the cells and to establish data for the scale-up of battery designs. In Battery B7-S [two Type B (thick) Li-Al/FeS cells in series], combinations of discharge/charge rates and equalization times were studied to establish specific energies at different deep discharge rates to a 1.0-V cutoff. At the 5-hr discharge rate followed by a 6-hr bulk charge and 4-hr equalization charge, a specific energy of ∿42 W-hr/kg was obtained over 36 cycles. Battery B9-S [two Type A (thin) Li-Al/FeS cells] was tested to study the problems associated with start-up and conditioning of cells in series. Because of initial cell resistances, a 25% reduction in the current normally used for start-up and conditioning promoted the break-in of the cells. Testing of Battery B9-S [two Type A (thin) Li-Al/FeS_2 cells in series] was directed at an evaluation of the effects of interspersing shallow cycles between the deep cycles. On deep cycling after a number of shallow cyles, the battery showed a decline in energy efficiency (∿5%) with shallow cycling at the 2- and 4-hr rates, but no significant change at the 5-hr rate. The specific energy also showed this declining trend.

Testing of Battery B7-S has continued for over 4152 hr and 225 cycles, with a specific energy of about 42 W-hr/kg at the 5-hr rate. Battery B9-S is achieving a specific energy of 46 W-hr/kg at the 5-hr rate after 744 hr and 66 cycles. Battery B8-S yielded a specific energy of about 38 W-hr/kg after 2250 hr and 378 cycles; this test has now been terminated to determine the cause of increasing cell resistance.

Battery Charging Systems

Detailed measurements of the prototype six-cell charge-equalization units developed by Gulton Industries, Inc. have shown that they meet all the design specifications. The successful operation of these units is a significant milestone in showing that cell equalization can be effected with a simple, lightweight system that shows promise of being economical.

A six-cell monitor/controller unit, that monitors individual cell voltages and terminates the charge or discharge when any cell reaches a preset cutoff voltage, is now operational; another unit is under construction.

Cell Development and Engineering

This part of the program is directed toward the development and testing of Li-Al/FeS_x cells having improved performance and lower cost. The work is concentrated on the development of cells that are adaptable to the electric vehicle.

Uncharged cells with hot-pressed FeS_2 electrodes are being developed for the electric-vehicle application. Two cells of this type, R-23 and R-24, have been placed in operation. In Cell R-23 the negative electrodes are plaques of pressed aluminum wire, whereas in Cell R-24 the negative electrodes contain Li-Al alloy in the pressed aluminum wire, a portion of which then serves as a current collector. At a discharge current density of 100 mA/cm^2, the respective utilizations and capacities were 53% and 55 A-hr for Cell R-23, and 83% and 93 A-hr for Cell R-24. The higher performance of Cell R-24 is attributed to better current collection in the negative electrode in which a part of the pressed aluminum wire acted as a current-collecting matrix.

Carbon-bonded positive electrodes using FeS or FeS_2 as the active material continue to show promise. Cell KK-5, an uncharged Li-Al/FeS-Cu_2S cell, has lost only 5% of its peak capacity after 5600 hr and 320 cycles. Cell CB-1, a charged cell with a carbon-bonded $CuFeS_2$ electrode, has accumulated 7800 hr and 562 cycles with 7% decline in capacity at the 5-hr discharge rate during the last 6000 hr. A large-scale cell (25 x 35 cm) with a carbon-bonded FeS-Cu_2S positive electrode has been operated for 2000 hr and 92 cycles, and has achieved 69% of the theoretical capacity at the 10-hr discharge rate with a coulombic efficiency of 99%.

Materials Development

The addition of a third metal to the Li-Al alloy negative electrode to prevent or minimize capacity decline is being investigated in engineering-size (13 x 13 cm) Li/Li-Al cells (the FM series). Additions of indium showed a beneficial effect; any favorable effects from calcium addition slowly disappeared.

The use of solid Li-Al alloy plaques, with low lithium content, as negative electrodes in uncharged FeS_2 cells has shown promise. Two uncharged Li-Al/FeS_2-CoS cells with BN felt separators have achieved specific energies of 100 W-hr/kg at slow discharge rates of 10 and 14 hr, respectively.

The corrosive environment within Li-Al/LiCl-KCl/FeS_x cells precludes the ready adaptation of most commercially available electrical feedthroughs. Improvements have been made in the Conax compression-type feedthrough by replacing the lower BN insulator with a stronger one of Y_2O_3 and by eliminating the massive compression nut by crimping the housing around a metal ring. This arrangement permits the use of a secondary solder-glass seal above the primary BN powder seal, thus decreasing the leak rate by about 10^4. This modified Conax feedthrough has proved to be reliable in all ANL and commercial cells. An effort is in progress to develop a solder-glass seal that can be used with molybdenum as well as iron current collectors.

Paper and felt separators are being developed as alternatives for the BN fabric that is currently used in Li-Al/LiCl-KCl/FeS_x cells. Tests conducted on a Y_2O_3 felt electrode separator with a 325-mesh screen over each electrode face showed that this is an effective separator-retainer combination. An effort has been initiated on the development of powder separators using Y_2O_3 powder with a particle size range of 150-250 μm. A cell with this type of separator was operated 200 hr with very good electrical performance. Other powders such as AlN, MgO and CaO are under consideration for use in powder separators.

Porous, monolithic ceramic plates are under consideration as alternatives to BN fabric separators. The following approaches to fabricating these plates are being evaluated: foaming techniques, alteration of the surface morphology of the particles, and the use of transient pore formers.

Current collectors in the positive electrode are exposed to metal sulfide and molten LiCl-KCl eutectic, a condition that results in rapid attack on most commonly used metals. Thus a number of metals have been subjected to corrosion tests in mixtures of LiCl-KCl with FeS and with FeS_2 for 500 to 1000 hr at 400 to 500°C. A variety of metals, including molybdenum, nickel,

niobium, Hastelloys B and C, and several Inconels are compatible with the FeS system. Low-carbon steels have also been used in cells with only minor corrosion over the temperature range; Hastelloy B appears to be marginally acceptable at 400°C. The brazed feedthrough requires corrosion-resistant, high-integrity brazed joints between the ceramic insulator and the metallic components, conducting rod, and cell housing. To facilitate the formation of this joint, Coors Porcelain Co. has developed several processes for metallizing the surface of Y_2O_3 ceramics. These processes were evaluated by exposing metallized samples to mixtures of LiCl-KCl and Li-Al for 300 and 900 hr at 450°C. The results of these initial tests are encouraging.

Postoperative examinations were continued on cells produced by ANL and by the industrial contractors. Chemical analyses of samples from five vertical prismatic cells have shown that sulfur is distributed fairly homogeneously throughout the positive electrodes and that no significant settling of the active material had occurred. No cross-contamination between the positive and negative electrodes was evident. However, recent examinations of Li-Al/FeS_2 cells have revealed the presence of Li_2S in BN fabric and felt separators. The Li_2S is crystalline and is accompanied by precipitated metallic iron particles. The mechanism involved in the deposition of the Li_2S is not known, nor has the effect of these deposits on cell performance been determined. Careful examinations of FeS cells have shown no evidence of Li_2S in the separators.

Among eight prismatic cells of various types that were subjected to postoperative examination, six had failed because of short circuits. The short circuits had several different causes: deposition of copper in the separator of an FeS-Cu_2S cell, extrusion of active material from either the positive or negative electrode, and displacement of current collectors as a result of electrode swelling. Operation of the other two cells, which both had FeS_2-CoS_2 positive electrodes, was terminated because of declining capacity.

Cell Chemistry

The discharge of FeS electrodes in the presence of LiCl-KCl eutectic electrolyte leads to the formation of Li_2S and iron at full discharge. A detailed study has been conducted on the reactions that occur during the discharge of the FeS electrode. Apparently, the discharge occurs by two paths involving the conversion of FeS either to Li_2FeS_2 or "J-phase" ($LiK_6Fe_{24}S_{26}Cl$), followed by the reduction of these two phases to Li_2S and iron. The addition of 9 mol % NaCl to the LiCl-KCl eutectic electrolyte appeared to improve the kinetics of the J-phase reduction, which may be a rate-limiting step.

To provide a better thermodynamic description of the system, emf measurements are being made on the Li-Al/FeS_2 couple as a function of temperature and state of discharge of the FeS_2 electrode. At 427°C the emf for the upper voltage plateau is 1.764 V with a temperature coefficient of 0.35 mV/°C, and that for the lower plateau is 1.327 V with a temperature coefficient of -0.16 mV/°C.

Studies were conducted on a variety of transition-metal sulfides as possible alternatives to FeS or FeS_2 in positive electrodes. Small cell tests indicated that TiS_2 and NiS_2 are promising candidates. Another study

indicated that Li_2S contamination of the Li-Al electrode has little effect on its performance.

A much higher specific energy than that of the present lithium/iron sulfide cells would result if liquid lithium electrodes could be developed successfully. The present studies have been aimed at maintaining preferential wetting of stainless steel substrates by the liquid lithium in the presence of molten-salt electrolyte. A Li-1.2 at. % Cu/LiF-LiCl-KCl/FeS cylindrical cell was constructed on the basis of the wetting study. This cell has operated for more than 60 charge-discharge cycles with no evidence of short circuiting or dewetting; however, its capacity is only 25 A-hr. Other cell designs are being considered.

Advanced Battery Research

Thermodynamic calculations were recorded for a variety of transition-metal sulfides to estimate the voltages, specific energies and overcharge potentials of cell systems using these materials in the positive electrode.

Metal oxide electrodes are being considered for use in secondary molten-salt cells. Thermodynamic calculations and cell tests were conducted on oxide positive electrodes. Calcium ferrate ($Ca_2Fe_2O_5$) appears to be a promising positive electrode for use with a calcium-alloy negative electrode. Of the various calcium-alloy electrodes that have been tested (Ca-Mg-Si, $CaMg_2$, $CaAl_2$, Ca-Al-Ca, and Ca_2Si), the Ca-Mg-Si system has shown the best performance characteristics.

Two engineering-scale ($\sim$60 A-hr capacity) Ca-alloy/FeS cells have been operated. A $CaAl_2$/FeS cell was operated for 1500 hr and 53 cycles. It had a high coulombic efficiency until the temperature was raised from 482 to 498°C; the higher temperature apparently caused the formation of a liquid metal phase in the negative electrode. Operation of a Ca_2Si/FeS cell at 500°C was terminated after 20 cycles because of a short circuit caused by leakage of active material from the positive electrode.

Cell and Battery Development at Atomics International

Several small cells with Li_4Si negative electrodes, FeS positive electrodes and LiCl-KCl electrolyte were tested. Four types of separator materials were used. These included BN cloth; rigid, porous AlN and Si_3N_4 plates; and a separator made by packing AlN powder in a cavity between adjacent electrodes. The last has yielded the most promising results. Work is in progress on porous rigid separators of β-Si_3N_4 and AlN, which are being scaled up to 23 x 23 cm (9 x 9 in.).

A 1-kW-hr multielectrode Li_4S/FeS cell has completed 3430 hr and 232 cycles; cell performance was excellent for 150 cycles, but declined steeply thereafter. An instrumented 1-kW-hr cell is being constructed for thermal characterization studies.

I. INTRODUCTION

Lithium-aluminum/metal sulfide batteries are being developed at Argonne National Laboratory (ANL) for use as (1) power sources for electric vehicles and (2) stationary energy storage devices for load-leveling on electric utilities, and storage of electric energy produced by solar, wind, or other sources. The performance goals for the electric vehicle batteries and stationary energy storage batteries are listed in Table I-1. These goals are the same as those given in the preceding report (ANL-76-98). Future revisions of these goals may be anticipated, however, as a result of further determinations of the requirements for these applications

Table I-1. Performance Goals for Lithium-Aluminum/Metal Sulfide Batteries

	Electric Vehicle Propulsion		Stationary Energy Storage	
Battery Goals	Mark I 1978	Prototype 1985	BEST 1981	Prototype 1985
Power				
Peak	30 kW	60 kW	1.5 MW	25 MW
Sustained Discharge	12 kW	25 kW	1 MW	10 MW
Energy Output	30 kW-hr	45 kW-hr	5 MW-hr	100 MW-hr
Specific Energy,[a] W-hr/kg	110	180	60-80	60-150
Discharge Time, hr	4	4	5	5-10
Charge Time, hr	8	5-8	8	10
Cycle Life	300	1000	1000	3000
Cost of Cells, $/kW hr	-	35	25-30[b]	20

[a]Includes cell weight only; insulation and supporting structure is approximately 25% of total weight for the Mark I electric vehicle battery and 15 to 20% for the 1985 prototype vehicle battery.

[b]Projected cost at a production rate of 2000 MW-hr/yr.

Because of the markedly different requirements for these two battery applications, a clear distinction is being made in the design characteristics of the cells being developed for the electric vehicle and stationary energy storage batteries. Table I-1 shows near- and long-term goals for each of the two batteries. The Mark I electric vehicle battery, which is the first full-scale battery of this type, will undergo experimental testing first in the laboratory and later in a van. The near-term stationary energy storage battery is scheduled for testing in the Battery Energy Storage Test (BEST) Facility in 1981. The goals for the 1985 prototype batteries for both applications are those considered necessary to meet the performance and cost requirements for commercial application. These goals were discussed in greater detail in the preceding report (ANL-76-98).

The differences in the near-term goals for the two applications may be summarized briefly as follows. The Mark I electric vehicle battery will have small cells of moderate cycle life, high specific energy, and high specific power, without cost restrictions. The cells for the BEST Facility battery can have moderate specific energy and specific power, but they must have a long cycle life and low cost at moderate production rates. The long-term goals require larger battery systems having higher performance and longer lifetime together with economically realistic production costs.

The battery development program includes both an in-house effort at ANL and contracts with several industrial firms to develop and fabricate electrodes and cells, electrode separators, electrical feedthroughs and battery components. Some general research and development work is also performed under contract. The contractors' efforts are closely coordinated with one another and with the base technology development at ANL.

In November 1976, the organization and management structure of the battery program at ANL was modified again to meet the changing needs of the program. These changes are reflected in the management structure of the program and in the organization of the report. The title of the report has been changed slightly to imply that stationary energy storage batteries are not necessarily limited to utility lead-leveling applications.

II. COMMERCIAL DEVELOPMENT
(A. A. Chilenskas)

The objective of the commercialization effort is the establishment of a competitive, self-sustaining industry capable of producing a supply of lithium/metal sulfide batteries that meets national needs. This objective is to be accomplished through normal market forces, with a minimum of governmental support. A commercialization plan is under development that will define the essential elements, *i.e.*, the market, product, and need (driving force for change). An essential part of this plan, the market study, has just been initiated; ANL is leading the study and assistance is being given by several industrial participants. The study will be a combination of a market survey and an economic analysis. The market survey will identify high-performance battery needs in military, aerospace and industrial applications for the near term (1978-1985) and will include existing and unfilled needs. The economic analysis will permit a projection of (1) the required production of lithium/iron sulfide batteries to satisfy the market for each year and (2) the capital expenditure requirements to support these production rates. In this way, the near-term markets will be used to build an industrial manufacturing base with a minimum of federal support.

A. Commercialization Studies

A commercial development plan that consists of a market study, an analysis of battery cost as a function of production rate, a manufacturing plan, a financial plan, and an analysis of competing technologies has been initiated.

The first phase of the market study was started in October 1976,* with assistance being given by three battery firms (Gould Inc., Eagle-Picher Industries, Inc., and the Atomics International Division of Rockwell International); these firms are currently industrial participants in the ANL battery program. The market study is directed toward the identification of target markets for the first commercial pilot-scale manufacturing facility for lithium/iron sulfide batteries. The study examines the potential of high-cost, low-volume markets for high-performance batteries in the cost range of about $100-200/kW-hr during the time span 1981-1985. Preliminary information indicates that these markets may support several plants with a battery production capacity of 100-200 MW-hr/yr.

B. Systems Design

1. Development of High-Efficiency Thermal Insulation for Electric-Vehicle Batteries

a. Requirements for Energy-Efficient, High-Temperature Electric-Vehicle Batteries
(A. A. Chilenskas)

An estimation of the energy efficiency of a high-temperature battery must include consideration of the energy required to maintain the battery at operating temperature, as well as the energy required to recharge. The energy required to maintain the battery temperature may be provided by electrical heaters within the battery housing, using an external source of electrical energy, the stored electrical energy of the battery, or the "waste" heat that is generated inside the battery during discharge and charge by the cell and connector resistance. The battery energy efficiency is thus a function of the battery resistance, the duty cycle (miles driven in the case of an electric vehicle), and the heat loss of the battery, as governed by the efficiency of the thermal insulation and such cooling as may be utilized to prevent excessive temperature generation. In addition, heat may be extracted from the battery with the battery coolant and used to heat the passenger compartment.

Calculations have been completed that relate the efficiency of batteries for two types of automobiles to the miles driven per year and the amount of heat lost through the battery insulation during the year. The calculations were based on the following assumptions: (1) the conversion of electrical energy during charging to electrical output during discharge is 70%, (2) the battery output required for each car is 0.12 kW-hr/tonne-km, (3) the heat loss is either 50 or 100 W for a compact car weighing 1270 kg (2800 lb) and is either 100 or 200 W for a 1820-kg (4000-lb) family-sized car, and (4) the heat generated within the battery is used to maintain the battery temperature by allowing the battery temperature to rise except when excess heat is available for comfort heating.

Battery efficiency can be expressed as

$$\text{Eff} = \frac{0.7\ E_B \times 100}{E_B + E_{IN} - 0.3\ E_B}$$

*This study was headed by S. H. Nelson of the Energy and Environmental Systems Division of ANL.

where E_B is the electrical energy delivered to the battery by the charger and E_{IN} is the total heat loss through the battery insulation during the year.

The results of the calculations are plotted in Fig. II-1. The energy efficiency is shown as a dotted line at values above 70% to indicate that a maximum of 70% of the charge energy is converted to electrical output and values greater than 70% represent the use of excess battery heat for passenger-compartment heating. Efficiency values less than 70% indicate that electrical energy in addition to that used for charging the battery must be supplied to maintain the battery temperature. The cost of maintaining the battery at operating temperature, assuming a cost of 5¢/kW-hr for electrical energy, is also shown in Fig. II-1.

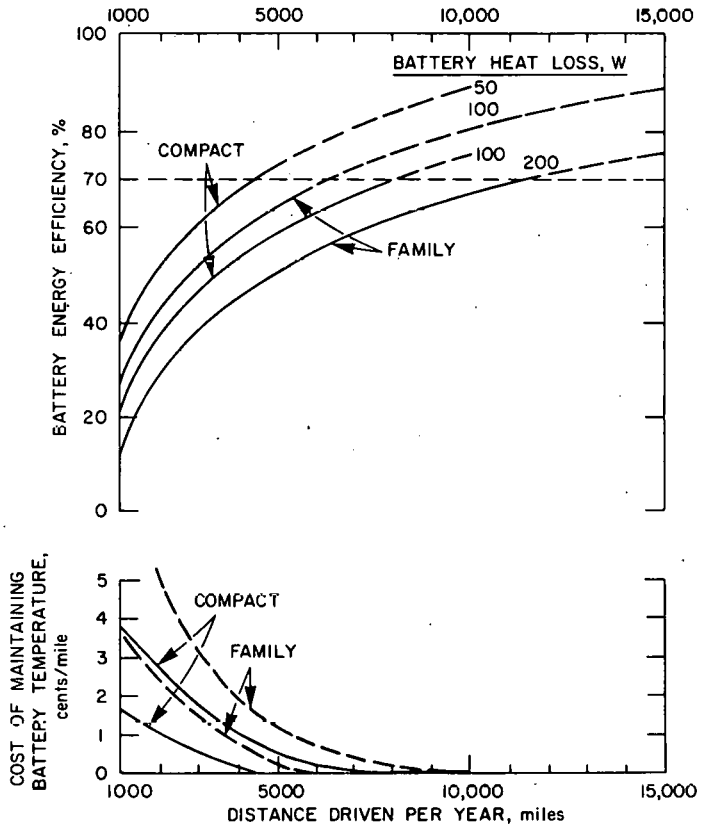

Fig. II-1. Energy Efficiency of Lithium/Iron Sulfide Batteries as a Function of Battery Heat Loss and Distance Driven

The results of these calculations lead to the following conclusions:

(1) The energy efficiencies of both batteries are very sensitive to the miles driven per year and the battery heat loss. A compact car with a battery heat loss of 100 W needs to be driven 13,000 km (8000 miles) per year to achieve a battery efficiency of 70%, but only 6400 km (4000 miles) per year if the battery heat loss is reduced to 50 W. Similarly, a family-

sized car with a battery loss of 200 W needs to be driven 19,000 km (12,000 miles) per year to obtain a battery efficiency of 70% and only 9700 km (6000 miles) per year with a battery heat loss of 100 W.

(2) The cost of maintaining the battery temperature can be reduced to zero for automobiles that are driven about 6000-10,000 km (∿4000 to 6000 miles) per year if the batteries are well insulated. For automobiles that are driven less, the cost of battery-temperature maintenance is still very small relative to other operating costs. For example, a compact car driven only 4800 km (3000 miles) per year would cost 0.9¢/km (1.5¢/mile), or $30/yr for battery-temperature maintenance with a battery heat loss of 75 W.

(3) From these considerations, appropriate heat-loss goals appear to be 75-100 W maximum for a compact car battery of about 30 kW-hr capacity and 150-200 W for a family-sized car battery of 50 kW-hr capacity.

b. Theoretical Considerations in the Application of Vacuum-Foil Insulation
(S. M. Ziv)

Thermal insulation, consisting of many parallel reflective radiation shields of metal foil in an evacuated space between the hot and cold surfaces, has been shown to be highly effective for high temperature applications. Because vacuum-foil insulation is being considered for use in battery systems, the fundamentals governing its selection and use are being reviewed.

Vacuum-foil insulation is inherently anisotropic in its heat conduction characteristics. It has a high thermal resistance normal to the surfaces of the radiation shields; the resistance parallel to those surfaces is lower by many orders. Because of the complexity of the analysis of corners and penetrations involving both normal and parallel (lateral) heat transfer, only normal heat transfer has been addressed in the present application.

For the normal direction only, there are three modes of heat transfer which are approximately additive:

(1) Radiation from shield to shield, involving numerous specular reflections of radiant energy back and forth in the space between adjacent shields.

(2) Gas conduction between adjacent shields, the magnitude of which depends on the degree of vacuum that is maintained.

(3) Solid conduction through the spacer devices that separate adjacent foils or, in the absence of such devices, solid conduction at points of contact between adjacent foils.

The relative importance of the solid-conduction mode depends on the specific design, whereas radiation and gas conduction can be considered as general phenomena, the study of which can define limits for certain parameters (*e.g.*, gas pressure and number of radiation shields). To achieve a low thermal conductance by the gas-conduction mode, the gas pressure must be low enough

that the mean free path of the gas molecules is much larger (a factor of 10 or more) than the space between adjacent shields. If this condition prevails, free molecular conduction is said to exist, and the heat flux is proportional to the pressure, and is independent of the space between the shields.

The radiation heat flux is essentially inversely proportional to the number of shields interposed between the hot and cold walls, and is directly proportional to the emissivity of the surfaces of the shields. An emissivity of about 0.05 appears reasonable for available metal foils (*e.g.*, aluminum) at the temperatures present in the battery enclosure.

The analysis showed that the effects of gas conductivity can be made small, relative to the effects of heat transfer by radiation, by maintaining the vacuum-foil insulation at pressures below ∿0.1 Pa (10^{-3} Torr). Heat transfer by radiation can be reduced to approximately 10 W/m^2 (∿1 W/ft^2) through the use of 30 to 40 reflective shields with an emissivity of 0.05. Since commercial vacuum-foil insulation is available with up to 50 or so shields per centimeter of thickness, a thickness of 1 cm or less should limit the heat transfer by radiation to about 10 W/m^2 (∿1 W/ft^2).

c. Evaluation of Vacuum-Foil Systems

(A. A. Chilenskas, J. E. A. Graae*)

Calculations were completed on the theoretical limits of heat loss in vacuum-foil systems to permit a comparison with experimental values, and thereby provide a basis for an estimate of the potential for further heat-loss reduction. Earlier work at ANL in 1970[1] had shown that a small cylindrical can at 400°C, insulated with 1 cm of Linde† vacuum-foil insulation, had a heat flux of 70 W/m^2 (6.5 W/ft^2). Using this value, the insulation thicknesses required to meet the proposed vehicle battery goals were calculated for two reference batteries. The results appear in Table II-1.

*Consultant to the Chemical Engineering Division of ANL.

†A division of the Union Carbide Corp.

Table II-1. Heat Loss of Typical-Size Electric Vehicle Propulsion Batteries

Type of Car Battery	Battery Surface Area, m^2	Insulation Thickness, cm	Heat Loss[a] through Foil, W	Total Battery[b] Heat Loss, W
Compact (30 kW-hr)	1.4	1.0	100	125
		2.0	50	75
Family (50 kW-hr	2.8	1.0	200	250
		2.0	100	150

[a] 70 W/m^2 for 1-cm thickness.

[b] A 25-W allowance for penetrations such as bus, cooling lines, etc. is allowed for the compact car battery and 50 W allowance for the family-sized car battery.

It can be seen from this table that an insulation thickness of about 2 cm is required if the heat loss is taken as that demonstrated in 1970, *i.e.*, 70 W/m^2. As shown in the preceding subsection, the potential for reducing the heat loss in vacuum-foil systems exists and it appears likely that insulation thickness of about 1 cm can be developed that will meet the goals set for electric-vehicle batteries.

Figure II-2 is a schematic diagram of a vacuum-foil insulated jacket manufactured by Linde that is being prepared for use in a six-cell battery test. The vacuum-foil insulation consists of multiple layers of aluminum foil separated by thin layers of glass paper. Penetrations for the bus, thermocouple, and power leads are made through a fiberboard plug 15-cm (6 in.) thick mounted on a 3-mm (1/8-in.) thick steel plate. The plug is gasketed to permit the use of an inert gas atmosphere inside the jacket, should that be desired. Tests performed by Linde showed that the total heat loss of the jacket was less than 50 W with an internal jacket temperature of >450°C. Assuming that about one-half of the heat loss occurs through the end plug, the heat loss through the vacuum-foil insulation is about 40 W/m^2 (4 W/ft^2).

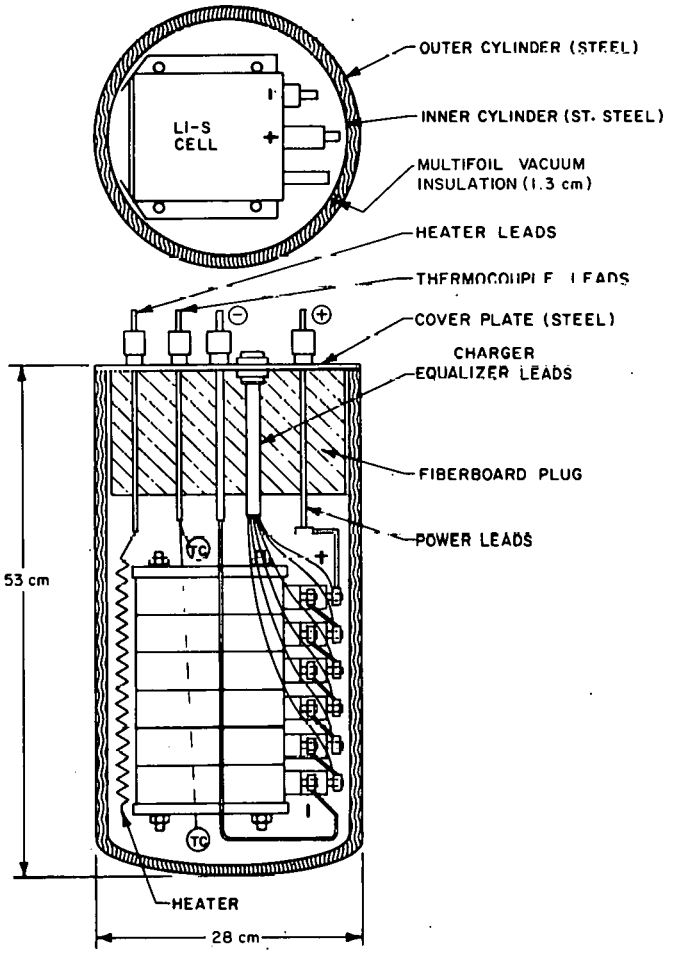

Fig. II-2. Insulated Jacket for Six-Cell Battery (In operation, the cells are oriented vertically.)

2. Conceptual Design and Cost Analysis of a Truckable Energy Storage Battery Module
(A. A. Chilenskas, J. A. E. Graae, R. F. Malecha)

A conceptual design/cost study of a truckable energy-storage battery module was initiated in December 1976 as a joint effort between the Chemical Engineering and Engineering Divisions of ANL. The design is to be sufficiently detailed to permit an analysis and cost estimate for the battery housing and auxiliaries.* This design will serve as the reference for the detailed design and construction of a truckable module of about 5 MW-hr capacity to be tested in the BEST (Battery Energy Storage Test) Facility. The BEST Facility is a joint undertaking by ERDA, the Electric Power Research Institute, and the Public Service Electric and Gas Company of New Jersey that will be used to test advanced batteries for utility energy storage plants. The lithium/iron sulfide battery module is expected to be ready for testing in the BEST Facility in 1981 or 1982.

The design concept is governed by the requirement to fabricate a battery housing as inexpensively as possible,† consistent with the technical requirements for this battery system. The design provides for construction and assembly in a semi-automated plant and is of such a size to permit delivery to a utility site via truck. Weather-tight construction is specified to eliminate the need for housing at the site. About 13 cm (5 in.) of inexpensive, commercially available insulation is adequate to maintain the proper battery temperature. Cooling to remove heat generated by battery inefficiency is provided by the use of once-through ambient air. Provision for the removal of cells without the need for cooling the module to ambient temperature is under study.

C. Industrial Contracts

1. Cell and Battery Development Contracts
(A. A. Chilenskas)

The effort in industry to develop manufacturing procedures and to design, fabricate, and test cells is continuing. This work is being carried out under contracts with Gould, Inc., Eagle-Picher Industries, Inc., and Catalyst Research Corporation.

Gould has completed the fabrication of six uncharged FeS cells (an Li_2S-iron mixture rather than FeS is used as the active material for the positive electrode) with hot-pressed, 13 x 18 cm (5 x 7 in.) electrodes. Four of these cells have been sent to ANL for testing and two were kept at Gould for testing. Efforts at Gould are now being directed to the design and fabrication of upper-plateau,‡ uncharged cells with 13 x 18 cm hot-pressed FeS_2 positive electrodes having molybdenum current collectors.

*The cost of cells manufactured in a production plant of about 1,150,000 kW-hr/yr of storage capacity has already been estimated and reported by W. L. Towle *et al.*[2]

†A preliminary target goal of $5-7/kW-hr of stored energy has been selected.

‡These cells are operated only on the upper of two voltage plateaus that are characteristic of FeS_2 cells.

The work at Eagle-Picher is directed toward the fabrication of 58 cells with 13 x 13 cm (5 x 5 in.) cold-pressed uncharged FeS electrodes. The cells are divided into nine groups with various design changes incorporated in each group; for example, variation in the ratio of positive to negative electrode capacity, increasing the diameter of the positive lead to 0.64 cm (1/4 in.) and the use of Y_2O_3 felt* rather than BN cloth† as a separator. Provisions for modifying the cold-pressing operation to increase the electrode size to 13 x 18 cm are under way.

At Catalyst Research, work is continuing on the development of procedures for the manufacture of cells in a dry air atmosphere. In addition, development work is in progress on the fabrication of Li-Al electrodes cast in metal substrates.

Eagle-Picher Industries, Inc. is also undertaking a design study of a housing for a 30 kW-hr electric vehicle battery, under a contract initiated in November 1976. This design study is a cooperative effort between ANL and Eagle-Picher, and is expected to lead to the design and fabrication of a prototype housing for the Mark I electric vehicle battery to be tested in a vehicle in 1978. The preliminary design is expected to be completed in February 1977 and fabrication of a full-scale prototype for thermal testing is scheduled for completion about September 1977.

2. Cell Materials and Component Development in Industry
(J. E. Battles, K. M. Myles, Z. Tomczuk, R. F. Malecha)

The development of cell components and selected materials by industrial firms is continuing. The present work is directed toward (1) the development of separator materials and the fabrication of these materials into usable separators, (2) the development of insulated feedthroughs, and (3) the production of materials of special importance to cell fabrication, *e.g.*, Li-Al alloys, LiCl-KCl salt, and Li_2S. The development effort at ANL on separators and feedthroughs is described in Section IV.A.

Carborundum Corporation is producing BN fiber for near-term use and is also conducting a design and cost analysis for a plant capable of producing BN fiber in large quantities. As part of a separate contract, Carborundum produced prototype paper separators using BN fiber bonded with BN; these were subjected to in-cell testing and appear promising. At the University of Florida,‡ a paper-making machine is being set up for a pilot-plant run to produce flat sheets of BN paper bonded with 10 wt % asbestos. This material will be used in engineering-scale cell tests. Work is in progress at Fiber Materials, Inc. on the development of a process for the manufacture of BN felt.

Ceramaseal, Inc. has developed a ram-type feedthrough that has exhibited excellent leak-tightness. Attempts are now under way to reduce the weight and size of the feedthrough. Coors Porcelain has developed a method of fabricating cold-pressed Y_2O_3 insulators and is working on a

*Produced by Zircar Products, Inc., Florida, N.Y.

†Produced by the Carborundum Corp., Niagara Falls, N.Y.

‡Funded directly by ERDA.

nonmetallic braze for Y_2O_3. The braze has been tested in materials compatibility experiments for up to 900 hr with satisfactory results.

A process for the production of Li_2S from Li_2CO_3 and H_2S has been developed by Eagle-Picher. The first five kilograms of product has been received and analyses have shown it to be >97% Li_2S.

3. Development of a Computer Controlled Electric Vehicle Load Profile Simulator

(F. Hornstra, J. Zagotta*)

An industrial participant contract with International Harvester on the development of a computer-controlled simulator for electric-vehicle load profiles has been completed. A computer program has also been developed to calculate the effects of variations in the control and power-train elements on the range and performance of electric vehicles powered by batteries.

The computer program simulates a battery-powered drive train with direct current motors having either series, compound, or shunt fields. Separate armature and field controls are provided for the latter two configurations. The program permits the use of various drive-line combinations such as a multispeed transmission with selectable gear ratios. One of the subroutines available for characterizing drive trains has a three-dimensional input to allow the efficiency to be specified as a function of both speed and torque.

Some sample runs were made using a hypothetical, light-duty delivery van conservatively characterized as follows: a 1500 kg (3300 lb) gross vehicle weight with a rolling resistance of 0.01, a drag coefficient of 0.004 kg/m^2 $(km/hr)^2$ or 0.002 lb/ft^2 $(miles/hr)^2$, a frontal area of 2.3 m^2 (25 ft^2), and a battery weight of about 430 kg (950 lb). Table II-2 shows a comparison of the driving ranges calculated for a Gould PB220 lead-acid battery and the projected 30 kW-hr ANL Li-Al/FeS_2 battery operating over the J227D driving profile with various motor, control, and drive-train combinations.

*Industrial Participant from International Harvester.

Table II-2. Calculated Ranges for a Light Delivery Van (1500 kg) Powered by a 430-kg Battery with Selected Motor/Control Systems Using a J227 Driving Profile

Type of Motor	Range, km (miles)							
	Electronic Chopper				Resistance Control			
	3-Speed Drive		Direct Drive		3-Speed Drive		Direct Drive	
	PB220[a]	Li/MS[b]	PB220[a]	Li/MS[b]	PB220[a]	Li/MS[b]	PB220[a]	Li/MS[b]
Series[c]	32 (20)	119 (74)	27 (17)	108 (67)	24 (15)	74 (46)	18 (11)	55 (34)
Compound[d]	29 (18)	113 (70)	29 (18)	114 (71)	29 (18)	97 (60)	21 (13)	71 (44)
Shunt[c]	34 (21)	113 (70)	26 (16)	64 (40)	34 (21)	105 (65)	24 (15)	56 (35)

[a]Commercially available lead-acid battery weighing 436 kg (960 lb).

[b]Li/FeS_2 battery weighing 432 kg (950 lb); output based on 1976 cell performance.

[c]Motor parameters obtained from a theoretical model.

[d]Motor parameters obtained from an actual motor.

Several observations about projected driving ranges can be made from the table. A three-speed transmission has little advantage over direct drive with either chopper-controlled series or compound motors, but with a shunt motor it provides an extension of range. With resistance-controlled motors of all configurations, the three-speed transmission provides a significant extension of the range over that for direct drive. For the Li-Al/FeS_2 battery, the resistance-controlled shunt motor with a three-speed transmission provides a range (105 km or 65 miles) that approaches that (113 km or 70 miles) achieved with a chopper-controlled unit with a three-speed transmission. Finally, the table shows that the calculated maximum achievable range with the Li-Al/FeS_2 battery is 119 km (74 miles) with a chopper-controlled series motor and three-speed transmission, compared with 34 km (21 miles) achievable with a lead-acid system having a shunt-controlled motor and a three-speed transmission.

Although most of the subroutines used in the computer program have not been quantitatively verified, the results of the simulated runs with the lead-acid battery are in reasonably good agreement with those published in road tests for similar batteries. Furthermore, one quantitative comparison has been documented. International Harvester conducted a test with a PB220 lead-acid battery and a compound motor using an electric driveline test stand having a dynamometer. The battery output measured in the International Harvester laboratory agreed very closely with the battery output calculated by the program.

III. BATTERY ENGINEERING
(E. C. Gay)

Battery engineering efforts are directed toward (1) testing of industrially fabricated Li-Al/FeS_x cells and batteries, and (2) improvements in electrode and cell designs and fabrication methods. As improvements in cell designs are demonstrated at ANL, these are incorporated into the industrially produced cells. Battery components and testing equipment are also being developed. A performance summary of cells and batteries is presented in Appendix A and Appendix B. Statistical data on the cell and battery tests are given in Appendix C.

A. Industrial Cell and Battery Testing
(W. E. Miller)

1. Testing of Contractor-Produced Cells
(R. C. Elliott, W. E. Miller, T. O. Cooper, P. F. Eshman, L. S. Kelley*)

A performance summary of contractor-produced cells is presented in Appendix A. Many of these cells are termed "baseline cells." These are cells that have been qualified by testing a series of cells of a set design to obtain baseline performance data. The baseline cell design is then used as a point of departure for testing the effects of various design modifications. Three baseline designs are currently being used: (1) thin-electrode Eagle-Picher cells (*e.g.*, the 1A series), (2) thick-electrode Eagle-Picher cells (*e.g.*, the 1B series), and (3) the present Gould design (*e.g.*, the 02 series).

*Industrial Participant from Eagle-Picher Industries, Inc.

a. Eagle-Picher Baseline FeS Cells

Testing of FeS_2 cells from Eagle-Picher was continued. The EP-2B3, -2B4, -2B5 series are assembled in the charged state. The electrodes in these cells are made by cold-pressing powders (Li-Al and electrolyte for the negative electrode and FeS_2, CoS_2 and electrolyte for the positive) into honeycomb current collector structures. The positive electrodes (half-cells)* are 0.63 cm thick and have a capacity of 78.0 A-hr. The volume fractions of materials in the positive electrode are 0.167 FeS_2, 0.022 CoS_2, 0.051 molybdenum honeycomb current collector, 0.702 LiCl-KCl electrolyte and 0.058 void. The negative electrodes are 0.72-cm thick and have a capacity of 78 A-hr. Volume fractions of materials in the negative electrodes are 0.63 Li-Al (48 at. % Li), 0.06 steel honeycomb current collector, 0.14 LiCl-KCl and 0.17 void.

Cells EP-2B4, -2B5 and -2B7 are essentially identical cells which were deep cycled (to a discharge cutoff voltage of about 1.0 V) at constant current (13 A, 42 mA/cm^2 current density) charge and discharge to test the effects of increasing the charge cutoff voltage. (Cell EP-2B4, one of the series, was also subjected to power tests; these results were reported previously in ANL-76-98, p. 16.) The results of the cycling tests for the three cells are shown in Fig. III-1. An increase in the charge cutoff voltage from 2.0 to 2.2 V increased the capacities of these cells from 80 A-hr (53% utilization of both positive and negative material) to 114 A-hr (76% utilization) for the stable period of operation. The stable period followed the

*Because the cells have two negative electrodes and one positive electrode, the positive electrode is considered to consist of two halves, each of the thickness indicated here. This dimension is referred to as the half-thickness.

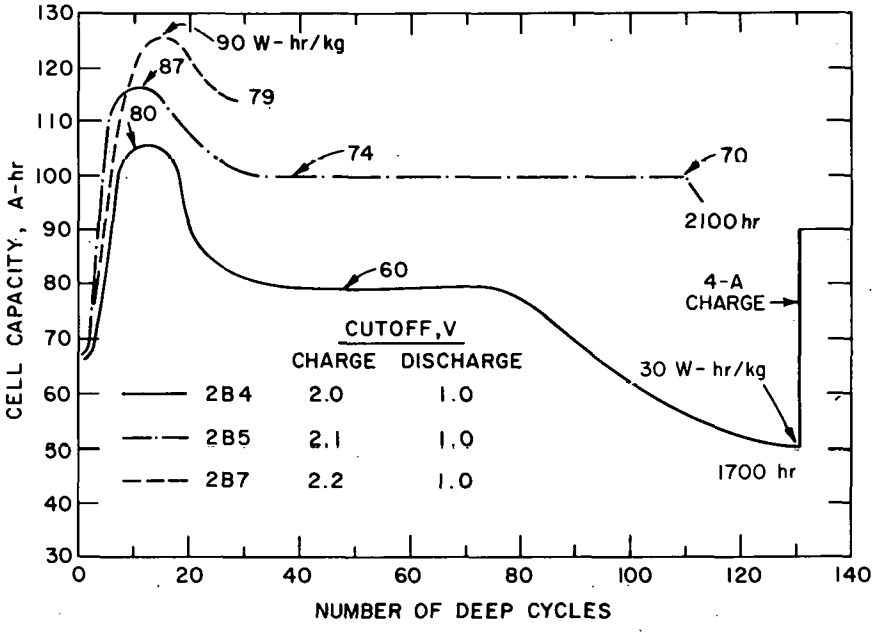

Fig. III-1. Cycling of Eagle-Picher Thick (Type B) Cells at 13 A (42 mA/cm^2)

period of peak capacity which occurred during the first 30 cycles. The specific energy increase that accompanied the increase in utilization was from 60 to 79 W-hr/kg.

Constant current cycling of Cell EP-2B4 was terminated after 1700 hr and 130 cycles because its capacity declined steadily after the 80th deep cycle. Much of the lost capacity of the cell was restored by reducing the charge current from 13 to 4 A; however, the regained capacity could not be retained on subsequent cycling at 13 A. The ampere-hour efficiency of this cell remained high (>98%) even at the end of its life. Testing of Cell EP-2B5 was terminated after 127 cycles and 2175 hr when its coulombic efficiency decreased markedly. Cell EP-2B7, after 30 deep cycles, was placed on the cycling schedule for electric-vehicle cells, shown in Table III-1. It has completed >1850 hr and >350 total cycles and is still operating well. Its specific energy is now 40 W-hr/kg at the 2-hr rate. This series of cell tests shows that reducing the charge cutoff voltage from 2.2 to 2.0 V had no effect on prolonging cell lifetime.

Table III-1. Seven-Day Cycling Schedule for Electric-Vehicle Cells

Cycle Number	Discharge Rate,[a] hr	Discharge Period, hr	Charge Period, hr
1 and 2	2	2	8
3 through 22	2	0.5	2
23 and 24	4	4	8
25 through 48	4	1	2

[a]Time required for a fully charged cell to reach 1.0 V at a set discharge current.

The construction of FeS_2 Type A (thin) cells is somewhat different than that of the Type B (thick) cells. The FeS_2 Type A negative electrodes are 3.25 mm (0.130 in.) thick with a capacity of 34 A-hr. The volume fractions of materials in the charged electrodes are 0.63 Li-Al (48 at. % Li), 0.09 current collector, 0.07 Al (added as powder to 48 at. % Li-Al), 0.12 LiCl-KCl electrolyte, and 0.09 void. (In the negative electrodes of the Type B cells, no free aluminum powder is added to dilute the Li-Al; the volume fraction of current collector is 0.06 and that of the salt plus void is 0.31.) The positive electrodes (half-cells) for the Type A cells are 3.25 mm (0.130 in.) thick and have a capacity of 35 A-hr. The volume fractions of materials in the positive electrodes are 0.138 FeS_2, 0.018 CoS_2, 0.062 current collector, 0.719 LiCl-KCl and 0.063 void. The compositions of the Type A and Type B positive electrodes are essentially the same.

Typical performance for Eagle-Picher Type A (thin) cells is reflected in the performance for Cell EP-2A5 (cycled at constant current of 10 A). The performance declined from an initial value of 66 W-hr/kg to

42 W-hr/kg after 200 deep cycles. These cells exhibit neither the dependence of capacity on charge cutoff voltage nor the peak capacity period during the first 30 cycles of the thicker cells described above.

b. Other Eagle-Picher Cells

The first cells produced by Eagle-Picher under an addendum to their contract have been received and testing has been started. The cell designs are variations of the FeS 1B design described previously (see ANL-76-81, p. 9). The purpose of these cells is to evaluate a number of proposed design changes for FeS cells. The first cell tested contained a separator of Y_2O_3 felt instead of BN fabric. Although it is recognized that Y_2O_3 may not be the most economical separator material for long-term use, it may serve satisfactorily as an interim material while other separator materials are being developed. Cell EP-I-1-A-2, which incorporated a Y_2O_3 felt separator, was tested to evaluate the effects of this change. Calculations indicated that there would be a minimal, probably immeasurable, difference in specific energy and specific power for a cell using a BN fabric separator and one using a Y_2O_3 felt separator of roughly the same thickness. Tests of cells with these separators indicate that this is the case.

The 13 x 13 cm cells with Y_2O_3 felt separators that have been tested to date (one ANL cell and two Eagle-Picher cells) have failed after 400-500 hr of operation. These failures may indicate that Y_2O_3 felt separators are not compatible with the present cell designs and fabrication procedures.

Plans have been made to test a variety of other experimental cells from Eagle-Picher during the next quarter. Variations in electrode thickness and porosity, minor changes in the mechanical cell design from the baseline Type A and Type B cells, and changes in the ratio of active materials in the negative and positive electrodes will be examined in these cells. All of these changes are directed toward producing more compact cells with higher specific energies.

c. Gould Cells

Gould Inc. delivered four Li-Al/FeS cells designed for stationary energy storage applications during the quarter. These cells consist of hot-pressed, uncharged electrodes which are 13 x 18 cm, 0.8 cm thick negative electrodes, and 0.5 cm thick positive electrodes. In two cells, calcium in the form of $CaCl_2$ was added to the negative electrode; the calcium was added with the aims of prolonging the life and improving the performance of the negative electrode. A number of tests will be required to optimize the negative electrode performance. The positive terminal feedthrough of these cells was developed as a joint effort between Gould and the ANL Materials Group. Cycling of these cells started at the end of the quarter.

2. Cell Heating and Cooling Experiments
(V. M. Kolba, J. L. Hamilton, G. W. Redding)

Temperature changes that occur during cell discharge and charge must be determined so that the heating and cooling requirements for the

battery design can be established. These temperature changes will influence the nominal operating temperature of the system, which must be kept within specified limits to avoid freezing of the electrolyte as well as excessive corrosion in the cell.

A preliminary experiment to measure temperature changes in an FeS_2 cell, described in ANL-76-81, p. 33, established that temperature changes occur during cell cycling. A second experiment is now being conducted. Eagle-Picher Cell 2B6 was instrumented with thermocouples, wrapped in a Briskeat* heater, overwrapped with Kaowool† insulation, and placed in a well equipped with a constant-power external heater. Baseline temperature data were obtained on this system prior to cycling. The cell was heated to a nominal temperature of 420°C by the external well heater. The cell temperature was then increased in stages by applying known amounts of power to the Briskeat heater. After the cell temperature was established at various heater power levels, the heater was turned off and the cell was started up and conditioned. (For a discussion of cell conditioning procedures, see Section III.A.4.b.) The cell is now being operated at various current levels and its temperature is being correlated with the state of charge, based on the cell voltage trace. Attempts are being made to correlate cell temperature changes with the entropic and resistive effects.

3. Cell Model
(R. C. Elliott)

A cell design model has been developed to evaluate the effects of design changes within the present cell systems on the specific energy and power of the cells. Calculations are now performed in a routine fashion, using the computer, for a large number of variations in cell design. Several significant conclusions have resulted from these calculations. The first is that the ratio of active material weight to total weight is still too low in the current cell designs. Since specific energy is inversely proportional to cell weight, a reduction of the latter is a requirement for improved performance. There is no single component in the cell whose weight can be trimmed sufficiently to achieve a dramatic increase in specific energy. However, there are numerous components that can be made slightly lighter to add up to a significant performance increase. A major factor in cell design is the extent of active material utilization in the electrodes. This item is treated empirically within the model as a linear correction factor on specific energy. In consideration of assumed utilizations and observed values, one can draw a general conclusion about electrode utilizations. The tendency to assume an optimistic utilization figure, design to it, and then not achieve it in practice should be avoided. It is much better to assume a conservative figure for electrode utilization and design the cell to that figure. Experimental measurement of utilization as a function of a number of variables is critical to the development of high-specific-energy cells. Future designs for the contractor cells will reflect the above considerations.

The cell model will be used as a cell specification-and-design tool in the development of the forthcoming Mark I electric-vehicle battery.

*Brisco Manufacturing Co., Columbus, Ohio.

†Babcock and Wilcox Co., Refractories Division.

4. Battery Testing

(V. M. Kolba, G. W. Redding, J. L. Hamilton)

Battery testing efforts are directed toward the development and evaluation of battery configurations and designs. In this effort, the performance of cells in series and parallel arrangements is being evaluated, start-up and conditioning methods are being investigated, and charging procedures and operational schemes are being developed. Testing of these battery configurations is under way, with FeS cells being tested for stationary energy storage applications and FeS_2 cells being tested for electric-vehicle applications.

Testing of cells in both parallel and series arrangements is required to fully understand the interactions of the cells and to establish data for scale-up of battery designs. In all present battery designs for both the electric vehicle and the stationary energy storage applications, cells are arranged in parallel-series configurations; the parallel connections provide increased capacity and the series connections provide increased voltage. To date, cells have been tested separately in both parallel and series arrangements. When a sufficient number of cells become available, testing will be conducted in combined parallel-series arrangements. Thus far, cells tested in this program have been individually monitored for voltage, and charge or discharge is terminated when one individual cell of the battery configuration reaches its voltage limit.

A description of the cells and batteries is given in Tables III-2 and III-3 together with information on life times and operational status. A summary of battery performance data is given in Appendix B. In the discussions of performance presented in this section, the specific energy and specific power values are calculated on the basis of combined cell weights.

Table III-2. Description of Cells Used in Battery Testing

Cell No.	Theoretical Capacity, A-hr	Type	Total Cycles	Total Operating Time, hr	Remarks
EP-1B4	149	FeS, thick	>289	>5337	Battery B7-S
EP-1B6	149	FeS, thick	>262	>4695	Battery B7-S
EP-2A3	69	FeS_2, thin	409	2736	Battery B8-S; terminated.
EP-2A4	69	FeS_2, thin	409	2736	Battery B8-S; terminated for post-test examination.
EP-1A7	69	FeS, thin	>66	>744	Battery B9-S
EP-1A8	69	FeS, thin	>66	>744	Battery B9-S

Table III-3. Description of Batteries

	Battery No.		
	B7-S	B8-S	B9-S
Cell Type	FeS (thick)	FeS_2 (thin)	FeS (thin)
Cell Designation	EP-1B4, -1B6	EP-2A3, -2A4	EP-1A7, -1A8
Total Operating Time			
Hours	>4152	2256	>744
Cycles	>225	379	>66
Status	Operating	Terminated	Operating

a. Testing of Thick FeS Cells

During this period, testing of Eagle-Picher Cells 1B4 and 1B6 in series (designated Battery B7-S) was continued. Combinations of discharge/charge rates and equalization times were investigated to establish specific energies at 4-, 5-, and 10-hr deep-discharge rates to a 1.0-V cutoff. For example, at the 5-hr discharge rate followed by a 6-hr bulk charge and 4-hr equalization charge, a specific energy of ∿42 W-hr/kg was obtained over a period of 36 cycles. Bulk charge refers to the first part of the charge period, in which most of the total ampere-hours are charged at high currents. This is followed by the equalization period, in which a small amount of charge is added at a very low current (<4 A). The cutoff voltages for both charge periods may be the same. Under these conditions, the decline in capacity and energy after 36 cycles was <6%, and over a period of 70 cycles the decline was <13%, to give a specific energy of ∿37 W-hr/kg. It was determined that a 50% saving in equalization time could be achieved by increasing the charge cutoff voltages for both the bulk charge and the equalization charge. The bulk charge cutoff was increased from 1.59 to 1.665 V and the equalization charge cutoff was increased from 1.58 to 1.65 V. The increased cutoff voltages resulted in an increase of ∿5% in capacity and specific energy over 14 deep discharge cycles. Testing at the 4-hr rate yielded a specific energy of ∿38 W-hr/kg; at the 10-hr rate the specific energy was ∿56 W-hr/kg. The battery is now being tested under a new cycling mode shown in Table III-4 to determine the effect of intermediate shallow cycles on subsequent deep cycles of the battery.

b. Testing of Thin FeS Cells

As discussed in ANL-76-98, p. 21, a method of start-up and conditioning of many cells prior to battery assembly and operation, is an important aspect of this program. With the advent of cells having similar initial resistances and with nearly equal capacities, a decision was made to reevaluate the problems associated with start-up and conditioning of cells in a series arrangement. The method was tested using two Type A (thin) Eagle-Picher FeS cells (Cells EP-1A7 and -1A8). The two cells were clamped together (using a mica separator in areas requiring electrical insulation), placed in a test well, started up, and conditioned in a series arrangement designated B9-S. Because of initial cell resistances, a 25% reduction in

Table III-4. Seven-Day Cycling Schedule for Energy-Storage Battery Cells

Cycle Number	Discharge Rate,[a] hr	Discharge Period, hr	Charge Period, hr
1 and 2	5	5	10
3 through 9	5	2	4
10 and 11	10	10	10
12 through 18	10	4	4

[a]Time required for a fully charged cell to reach 1.0 V at a set discharge current.

the current normally used for start-up and conditioning promoted the break-in of the cells. The coulombic efficiency was high (>98%) with good energy efficiency during the break-in and initial cycling. The specific energy of this battery was 49 W-hr/kg at the 10- and 7-hr rates, 46 W-hr/kg at the 5-hr rate, and 41 W-hr/kg at the 3-hr rate.

A comparison of the specific energies of the Type A (thin) FeS cells (B9-S) and the Type B (thick) FeS cells (B7-S) shows that the values attained with the thin-electrode cells compare very favorably and exceed those obtained with the thick-electrode cells at the 5-hr rate. However, at the longer discharge times (*e.g.*, 10-hr rate), the thick-electrode cells show their superior specific energy capability. Here again, as in the case of the FeS_2 cells, the advantage of thin electrodes for high-rate performance has been demonstrated. The battery is now being tested under the new cycling mode, described in Table III-4.

c. Testing of Thin FeS_2 Cells

During this period, testing of Battery B8-S (Eagle-Picher Type A FeS_2 Cells 2A3 and 2A4 in series) was directed to an evaluation of the effects of interspersing shallow cycles (0.5- to 1-hr discharge/charge cycles) between the deep cycles. This test was aimed at establishing shallow cycling modes and determining changes in performance caused by shallow cycling. For example, shallow discharges of 0.5 and 1 hr were conducted at the 2-hr and 5-hr rates. Half-hour discharges were also conducted at the 4-hr rate. Under the chosen conditions, the battery performance on deep cycling after a number of shallow cycles (minimum, 6 cycles; maximum, 49 cycles) showed a decline in energy efficiency ($\sim$5%) with progressive shallow cycling at the 2- and 4-hr rates, but no appreciable change at the 5-hr rate. The specific energy also showed this declining trend; however, the decline was larger, being about 20% at the 2-hr rate and about 8% at the 4-hr rate.

Power tests were conducted on Battery B8-S after about 2200 hr of operation. These data and the voltage data corroborate the observation of increasing cell resistance noted during the operating life. In general, the performance of the battery was good prior to termination of the test.

On the 378th cycle, at the 5-hr rate, the utilization (based on lithium) was about 58% with ∿99% coulombic efficiency and a specific energy of ∿38 W-hr/kg. The peak specific power (at the end of a 15-sec high-power pulse) at 5% discharge was ∿26 W/kg at a 50-A rate, while at 25% discharge it was about 23 W-hr/kg at the 50-A rate.

Testing of the battery was voluntarily terminated after 2256 hr and 379 cycles to determine the cause of the increasing cell resistance. One of the cells was submitted to the Materials Group for post-test analysis. The results of this analysis are discussed in Section IV.A.5 of this report.

B. Charging Systems for Electric Vehicle Batteries
(F. Hornstra, E. C. Berrill, T. Morgan*)

1. Gulton Equalizers

More detailed and careful measurements of the prototype six-cell equalizer units developed by Gulton Industries, Inc. showed that they did indeed meet the design specifications in every respect. The measurements were complicated by the nature of the current wave form. Square-wave current pulses of 50% duty cycle are generated by the equalizer. Diodes in the circuit provide rectification and of course block the cell from discharging back into the charger during the interval of time when the current is zero. Consequently, during that zero-current interval, the voltage at the cycler terminal decreases to the IR-free cell voltage. A measurement of the equalizer voltage with a dc meter gives a value which is the average of the voltage during the current pulse and the voltage during the zero-current interval. The value resulting from this measurement makes it appear that the equalizer is regulating the voltage with less compliance than is actually the case.

The correct way to evaluate the performance of such a system is to make instantaneous, coincident measurements of current and voltage during the current pulse. These measurements, when made with the use of a calibrated oscilloscope, verified that the units performed in accordance with the specifications.

The successful operation of these units is a significant milestone in demonstrating that cell equalization can be effected with a simple, lightweight system that shows promise of being economical. Such a system might be useful for virtually all types of batteries.

2. TRW Proposal
(F. Hornstra)

Representatives of TRW Inc. visited ANL in October to discuss a battery charging system for the Li-Al/FeS_2 electric-vehicle battery. As a result of this visit, they have submitted a proposal for a two-step development program leading to a complete charger suitable for use with an electric vehicle. The first step, which is addressed at length in the proposal, involves a design study to assess the requirements and establish design goals for a charging system that would be an integrated unit consisting of a bulk

*Co-op student from the University of Cincinnati.

battery charger functionally combined with a cell-equalization system. This study would conclude with a recommended charging system for a development and construction program under Phase 2 of this program. The proposal is currently under study.

3. Electronic Development
(F. Hornstra, W. W. Lark, T. Morgan*)

A six-cell monitor/controller is now operational and another unit is under construction. The monitor/controller monitors each cell voltage and terminates the battery charge process when any cell reaches a preset charge cutoff voltage and terminates the discharge process when any cell reaches a preset discharge cutoff voltage. Thus, the battery can be used to its fullest extent without exposing any of its cells to overcharging or discharging. Twenty-five "watch-dog" monitors have been constructed by the ANL Electronics Division and are ready for use; the delivery of the units completes this project. The "watch-dog" units can be used with any battery. The units operate independently of the charger or cycler. If the battery voltage exceeds a preset upper limit or declines below a preset lower limit as set on the "watch-dog," the battery is placed on open circuit. In this manner, a battery is protected from damage resulting from malfunctions of the charger or cycler system.

C. Cell Development and Engineering
(H. Shimotake)

The effort in this part of the program is directed toward the development and testing of Li-Al/FeS_x cells having improved performance and lower cost. Technical advances will be incorporated into the cells that are fabricated by industrial firms to complement the effort on industrial cell development. The work is concentrated on the development of cells that are particularly adaptable to the electric-vehicle application, with emphasis on high specific energy at the 2-hr and 4-hr discharge rates. A number of "upper-plateau" FeS_2 cell tests were initiated during this quarter. Efforts are also under way on the selection of an improved separator, investigations of the use of metal additives to Li-Al electrodes to extend electrode life, and the development of carbon-bonded electrodes. Dimensions of electrodes in the test cells are usually 13 x 13 cm, except for special-purpose cells. A summary of performance results of the test cells is presented in Appendix A.

1. Cell Performance and Lifetime Improvement

a. Uncharged Cells with Hot-Pressed FeS_2 Electrodes
(L. G. Bartholme and H. Shimotake)

Uncharged, upper-plateau FeS_2 cells have been selected for the near-term electric-vehicle application. These cells have several potential advantages over the two-plateau FeS_2 cells: (1) high average voltage, (2) a single voltage plateau (thus simple voltage control), (3) potentially good performance at high discharge rates, and (4) high energy efficiency. The disadvantages are (1) an intrinsic limitation of the capacity by the positive electrode material, and (2) insufficient design data at the present time.

*Co-op student from the University of Cincinnati.

A series of cell tests has been planned to characterize the upper-plateau FeS_2 cells. Objectives of the tests include (1) selection of an optimum cell design using available materials, and (2) determination of the performance characteristics of upper-plateau cells as a function of discharge rates, cutoff voltages, and Fe:S, Li:S, and Al:S ratios.

Two cells, R-23 and R-24, have been built and placed in operation. Both cells are prismatic (13 x 13 cm) and comprise a central hot-pressed positive electrode and two negative plaques of pressed aluminum wire, similar to those used in previous R-series cells (ANL-76-98, p. 26). The basic difference in the two cells is in the negative electrodes. In Cell R-24, the negative electrode contains Li-Al alloy, thus making a portion of the pressed aluminum wire the current collector.

The two cells have shown remarkable differences in their capacity and energy outputs, particularly at the high-rate discharges, as shown in Fig. III-2. At a 30-A discharge (current density, 100 mA/cm^2), the utilization and capacity of Cell R-24 were 83.2% and 93 A-hr, respectively; those for Cell R-23 were 53% and 55 A-hr, respectively. The superior performance of Cell R-24 over R-23 is attributed to the better current collection of the negative electrode of Cell R-24 in which a part of the pressed aluminum wire acted as a current-collecting matrix. Efforts to build and test more upper-plateau FeS_2 cells are continuing.

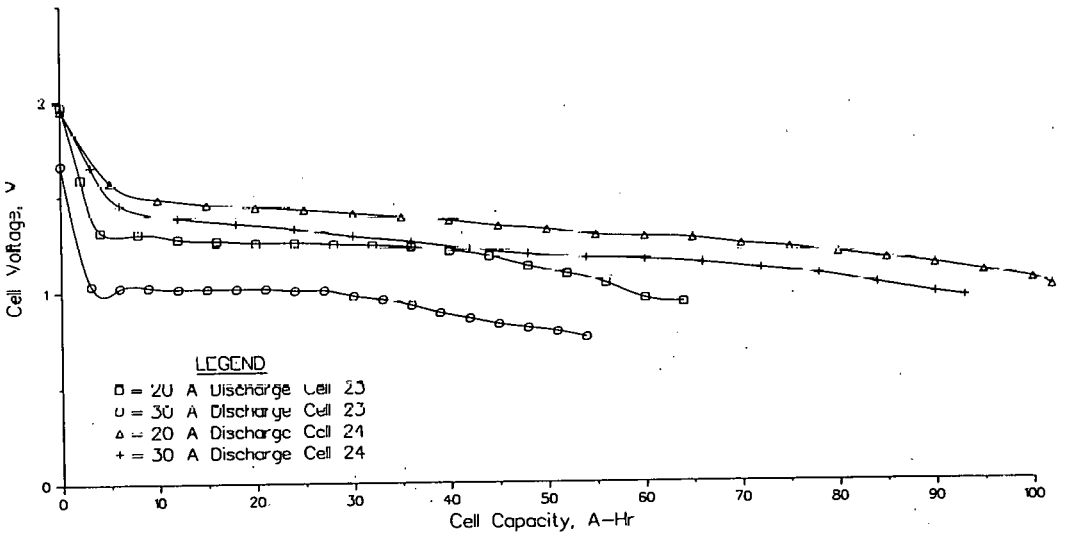

Fig. III-2. Voltage-Capacity Curves for Cells R-23 and R-24 (temperature, 450°C)

b. Carbon-Bonded Metal Sulfide Electrodes
(T. D. Kaun, W. A. Kremsner, F. J. Martino)

Recent developments of carbon-bonded electrodes have included the identification of a number of suitable carbon-binders. The use of furfural alcohol resin as a binder has resulted in improved electrode performance; phenol formaldehyde and Union Carbide grade C-34 binders also show promise.

At present, three cells, Cells KK-4, 5 and 6, with carbon-bonded positive electrodes are being subjected to lifetime testing. These are compact, sealed, prismatic cells operated at 450°C. Physical characteristics of these cells are given in Appendix A. Cell KK-5, an uncharged FeS cell with Cu_2S additive has retained most of its capacity after 320 deep-discharge cycles and 5600 hr. The peak capacity of 90 A-hr has diminished by only 5%. This recent decline in capacity corresponds to an increase of cell resistance from 3.8 to 4.8 mΩ. When the cell is charged at currents lower than those corresponding to the 10-hr rate, full capacity is restored. Therefore, with a more effective charging technique than the constant-current mode, *e.g.*, constant-voltage charging, Cell KK-5 should easily reach a goal of 400 cycles with <10% capacity decline. The cell capacity is also stable at high discharge rates. The specific energy at the 2-hr discharge rate (40 A) is greater than 45 W-hr/kg.

Cells KK-4 and KK-6, which have carbon-bonded FeS_2 electrodes, have operated for 350 and 280 cycles, respectively, with 98+% coulombic efficiency. Capacity declines thus far are 15 and 50%, respectively. The loss of capacity in these cells, unlike that of Cell KK-5, does not appear to be recoverable. Plans have been made to reconstruct one or both of these cells by inserting fresh negative electrodes to determine which electrodes are life-limiting.

Cell CB-1, constructed as an unsealed charged cell, was designed to test a positive electrode of carbon-bonded chalcopyrite ($CuFeS_2$) with hot-pressed pyrometallurgical Li-Al negative electrodes. This cell has now accumulated 562 cycles and 7800 hr of operation. During the last 6000 hr of operation, its capacity has declined <7% at the 5-hr charge-discharge rate (12.5 A, 65 mA/cm^2). Lowering the discharge current resulted in higher cell capacity, indicating that, even after this extended operating period, additional capacity is still available. Lowering the charge current resulted in a 2% rather than the 7% decline in capacity from its typically high 67 A-hr value (43% of the theoretical capacities of the negative and positive electrodes). Throughout the testing of Cell CB-1, the cutoff voltages have been maintained at 0.9 V and 1.75 V (IR included). Cell resistance has remained at ∿12 mΩ while the ampere-hour efficiency has varied between 92 and 98%.

2. Large-Scale Cell
(F. J. Martino, T. D. Kaun, J. E. Kincinas)

The operation of a 25 x 35 cm compact cell (SS-1) has been temporarily suspended in order to seal a lid on the cell. The cell contains a carbon-bonded FeS-Cu_2S positive electrode and negative electrodes of Li-Al in iron Retimet. The cell has been operated for 92 cycles and ∿2000 hr and has achieved capacities as high as 450 A-hr (540 W-hr) at a 10-hr discharge rate of 40 A. This capacity corresponds to 69% of the theoretical value. Also, the ampere-hour efficiency of the cell has remained at 99% throughout its operation.

Power testing of Cell SS-1 yielded typical power-pulse data for FeS cells with a peak specific power of 30 W/kg. A specific energy of 45 W-hr/kg was measured at the 10-hr discharge rate. Cell resistance has been constant at 1.4 mΩ.

3. Electrode Development

a. Li-Al Alloy Negative Electrodes with Additives
(F. J. Martino, H. Shimotake)

The addition of a third metal to the Li-Al alloy has shown promise in preventing capacity decline of small-size (15 cm^2) Li/Li-Al cells (ANL-76-98, p. 44). As a result, engineering-size cells (FM series) are being operated to test this concept. Each cell has a well defined Eagle-Picher Type A positive electrode, and a negative electrode in which pyrometallurgically prepared Li-Al and an additive are loaded in an iron Retimet* current collector. The charge-discharge current for these test cells, the IR-free cutoff voltages, and operating temperatures are all being held constant at 8.0 A, 1.05-1.70 V, and 450°C, respectively.

Cell FM-1, which has a negative electrode of Li-Al-4 wt % In (85 A-hr theoretical capacity), continues to operate after 210 cycles and 2460 hr. Although its overall performance has declined ~5% from a typical high of 45 A-hr, its ampere-hour efficiency has remained above 93%. Therefore, it appears that indium shows promise as a negative electrode additive to extend cell lifetime.

Cell FM-2, with a Li-Al-8 wt % Ca negative electrode of 90 A-hr theoretical capacity, began its operation with a higher capacity than Cell FM-1; early cycling showed an immediate rise to a peak capacity of 56 A-hr. However, continued cycling indicated that any beneficial effects from the calcium addition were slowly lost. Because of its poor performance after 128 cycles and 1775 hr, Cell FM-2 was taken out of operation and will undergo post-operative analysis.

Replacing Cell FM-2 in the negative electrode additive tests is Cell FM-3, which has a Li-Al-8 wt % Sn negative electrode of 82 A-hr theoretical capacity. This cell is still undergoing break-in cycling with only 6 cycles accumulated to date.

b. Cast Li-Al Alloy Negative Electrodes
(T. W. Olszanski, E. C. Chaney,† H. Shimotake)

The use of solid Li-Al alloy plaques, with low lithium content, as negative electrodes in uncharged FeS_2 cells has shown promising results. This type of negative electrode may provide the least contamination of the Li-Al alloy, since it eliminates the use of high-surface-area powders. The solid negative plaque can incorporate excess Li-Al alloy for added capacity or excess aluminum for added current collection.

Two cells, EC-1 and TO-3, having solid Li-Al negative electrodes, have been operated. Cell EC-1, a sealed cell with an uncharged FeS_2-CoS positive electrode, was operated for 25 cycles when the test was terminated because a short circuit had developed. This cell contained a BN felt separator with no particle retainer such as ZrO_2 cloth which has been used in the positive electrodes of many cells. This cell achieved a specific energy of

*A porous metal produced by Dunlop, Ltd., Coventry, England.

†Industrial Participant from Gould Inc.

approximately 100 W-hr/kg at the 10-hr rate. Cell TO-3, also a sealed cell with an uncharged FeS_2-CoS positive electrode, was operated for 6 cycles and 230 hr. Cell TO-3 also had a BN felt separator without a particle retainer. This cell attained a specific energy greater than 100 W-hr/kg at the 14-hr rate during initial cycling. The overall performance of Cell TO-3 at different discharge rates is presented in Fig. III-3. Further tests in this investigation will be directed toward determining the cause of short circuits in these compact, high-specific-energy cells.

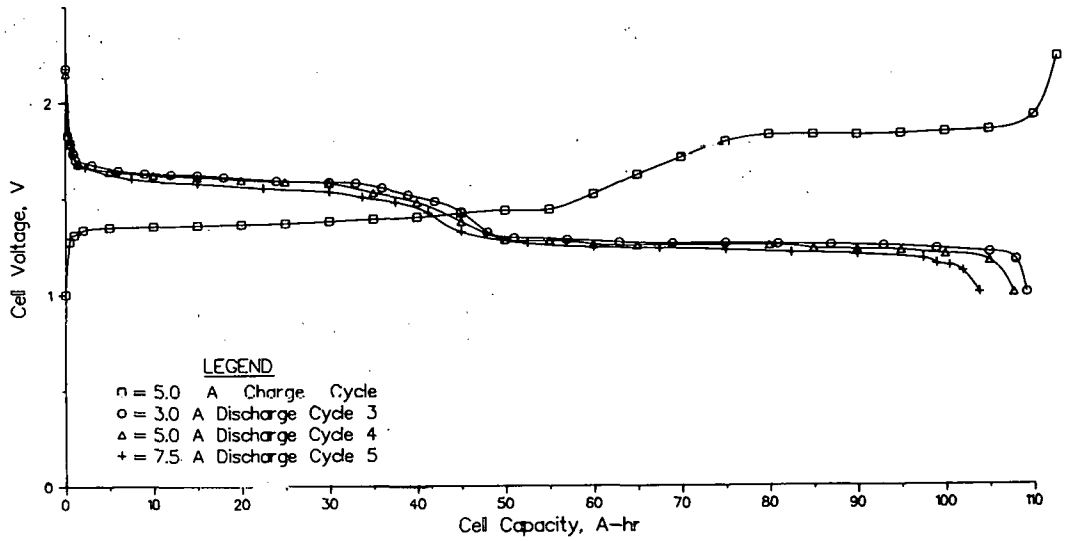

Fig. III-3. Voltage-*vs.*-Capacity Curves for Cell TO-3 (temperature, 430°C)

IV. TECHNOLOGY DEVELOPMENT

A. Materials Development
(J. E. Battles)

Efforts in the materials program are directed toward the development of various cell components (*e.g.*, electrical feedthroughs, electrode separators, current collectors, and cell hardware), corrosion testing of candidate materials for these components, and postoperative examination of cells to evaluate the behavior of the various construction materials as well as that of the lithium-aluminum and metal sulfide electrodes.

1. Electrical Feedthrough Development
(K. M. Myles and J. L. Settle)

The corrosive environment within Li-Al/LiCl-KCl/FeS_x cells precludes the ready adaptation of most commercially available electrical feedthroughs. The few that are compatible with the cell environment employ mechanical seals, such as the Conax electrical feedthrough, which do not adequately meet the technical goals of small size, light weight, low cost, and leak-tightness.

It has long been recognized that the best solution would be a brazed feedthrough, and new and innovative brazed seals are being sought with some success. However, work is also under way to minimize the shortcomings of the mechanical seal for near-term applications.

As previously reported (ANL-76-98, p. 33), this effort has resulted in a modified Conax feedthrough that has proved to be reliable in all ANL and commercial cells. During the past quarter, several significant improvements were made in the mechanical feedthrough. First, the lower BN insulator, which was relatively weak, was replaced by a substantially stronger insulator of Y_2O_3, with the result that the BN powder sealant can now be compacted much more tightly; in addition, new assembly specifications were established for a feedthrough with a conductor having a diameter of 1/4 in. (0.64 cm). Second, the feedthrough housing was redesigned to reduce the mass and to eliminate the massive compression nut by crimping the housing around a metal ring. This housing also allows a secondary solder-glass seal to be used above the primary seal of compacted BN powder. With this modification, crimp-type feedthroughs have been fabricated with leak rates as low as 10^{-10} Pa·m^3/s, which is a significant improvement over leak rates of 10^{-6} Pa·m^3/s without the solder glass. Comparative weights of the various components of the feedthrough are listed in Table IV-1; two sizes of insulators were fabricated, one to accommodate a 5/16 in. (0.79 cm) diameter conductor, the other a 1/4 in. (0.64 cm) diameter conductor.

Table IV-1. ANL Mechanical Feedthrough

	Component Weight, g, for Indicated Conductor Diameter, in. (cm)	
	5/16 (0.79)	1/4 (0.64)
Steel housing[a]	58	58
Y_2O_3 lower insulator	10	14
Al_2O_3 upper insulator	4	6
BN powder sealant	5	5
Steel retainer ring	2	2
Solder glass	1	1
Total	79	86

[a]Conax housing weighs 120 g.

Heretofore, the insulators for the crimp-type feedthrough were designed so they would also fit the Conax feedthrough housing to provide a back-up. The recent successes, along with the decision to scale down the thickness of the cells to 3/4 in. (1.90 cm) for the Mark I vehicle battery, led to a decision to scale down the feedthrough for the 1/4 in. (0.64 cm) diameter conductor to a maximum outside dimension of 3/4 in. Some uncertainty is incurred by the redesign in that the walls of the ceramic insulators are appreciably thinner and that the metal housing might creep excessively at the

cell operating temperature. Nonetheless, the redesign has commenced (see Fig. IV-1), and the ceramic insulators have been ordered.

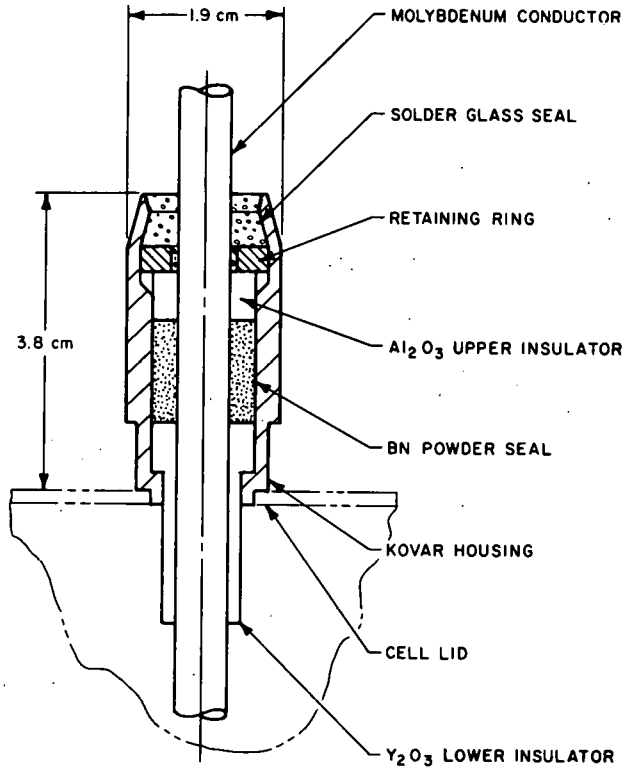

Fig. IV-1. Crimp-type Feedthrough for Mark I Electric Vehicle Cell

A facet of the effort that requires immediate attention is the development of the solder-glass seal for molybdenum current conductors; the previous development had involved iron conductors. This change does not represent a major departure, since the design criteria are less demanding for the molybdenum conductor. However, since Kovar* must now be used instead of steel for the housing material, some effort must be placed on an understanding of the metallurgy involved in welding the housing onto the cell lid, which is low-carbon steel.

2. Electrode Separator Development
(J. P. Mathers and C. W. Boquist)

Paper and felt separators are being developed as alternatives for the BN fabric which is currently used as the electrode separator in Li-Al/LiCl-KCl/FeS_x cells. The paper and felt separators are expected to be considerably less expensive than BN fabric and to provide more effective retention of the active materials in the electrodes. An effort has also been initiated to determine the feasibility of using electrode separators composed entirely of ceramic powders.

*Composition of Kovar (wt %): 54 Fe-29 Ni-17 Co.

The performance of Y_2O_3 felt as a particle retainer was evaluated in Cell SC-12. This was a Li-Al/LiCl-KCl/FeS cell which was assembled in the uncharged state. Yttria felt of 80-mil (2.0-cm) thickness was used as the separator, with a layer of 325-mesh screen over each electrode face. The design of the cell was similar to that shown in ANL-76-35, Fig. II-6, p. 20. In previous cells, however, ZrO_2 fabric had been used as a particle retainer for the active materials. Cell SC-12 was operated for 1300 hr (106 cycles) at a current density of 76 mA/cm^2. The electrical performance of the cell was very good throughout its lifetime. Operation of the cell was terminated when it failed to accept a charge after a shutdown period of 24 hr for cycler repairs. Post-test examination revealed an electrical short circuit in the cell which was not associated with the Y_2O_3 separator. Metallographic examination of a section through the cell showed that the separator had maintained its integrity during cell operation. There were some very small metal particles in the felt, but these were confined to a thin band close to the positive electrode. The remainder of the felt thickness (~80%) was free of any particulate matter. These results indicate that a combination of 325-mesh screen with a layer of Y_2O_3 felt can be used as an effective separator-retainer combination.

An effort to develop an all-powder separator was initiated this past quarter. Cell SC-13 was constructed with a separator that consisted of Y_2O_3 powder with a particle size range of 150-250 μm. The separator thickness was 4 mm. A diagram of the cell is shown in Fig. IV-2. Yttria powder was also used to insulate the sides and top of the FeS positive electrode from the cell housing. A 325-mesh screen was used over each electrode face for electrode particle retention. The cell was cycled continuously at a current density of 75 mA/cm^2 for 2000 hr before the operation was terminated voluntarily. The electrical performance of the cell was very good throughout the experiment. Post-test examination showed that a uniform separator thickness was maintained around the positive electrode. Microscopic examination of a section through the separator showed that some of the smaller Y_2O_3 particles had settled to the bottom of the separator. As a result, the bottom half of the separator was less porous than the upper half. Also, some of the fine particles from the positive electrode had filtered through the 325-mesh screen. These particles were retained in the upper 15% of the separator; the remainder of the separator was free of electrode particles.

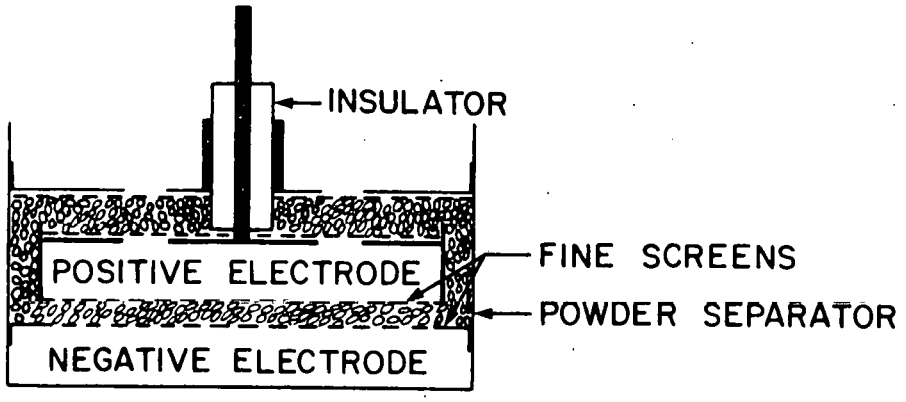

Fig. IV-2. Schematic Representation of Cell (SC-13) for Testing Powder Separator

The results obtained with the all-powder separator are very encouraging. The use of powder separators might make it possible to use materials such as AlN, MgO, and CaO, which are not available in fibrous form. A possible disadvantage of the powder separator is that it is less porous than a fibrous separator, and the lower porosity may restrict ionic transport through the separator. This effect could limit cell performance, especially at higher current densities.

Work on the all-powder separator is proceeding and experiments are now in progress in an attempt to reduce the separator thickness and to investigate the use of powder separators in alternative cell designs, such as the vertical prismatic design used in the industrially produced cells.

3. Ceramic Materials Development
(W. D. Tuohig and J. T. Dusek)*

Porous, monolithic ceramic plates are under consideration as alternatives to the BN fabric separator, and several approaches to fabricating these plates are being evaluated. Foaming is a particularly attractive approach because of the wide latitude in the structures that can be produced (ANL-76-81, p. 34). Yttria foams were prepared from aqueous suspensions of ceramic powder,† commercial foaming agents,‡ and organic binders in a high-shear mixer. Later, the foams were cast in shallow metal molds. The resulting plates were dried at low temperature (50-75°C) to prevent cracking and then cured by firing at temperatures between 1500 and 1800°C. Cured foams exhibited porosities in the range from 63 to 90% of the geometric volume, depending on the processing parameters used. A commercial foam generator** has been leased to facilitate further development of foamed separators. The generator combines air with aqueous solutions of foaming agents to produce a uniform foam matrix. Ceramic powders can then be mixed with this foam to produce any predetermined density.

A second approach to the fabrication of porous plates involves alteration of the surface morphology of the particles. Figure IV-3 is a scanning electron micrograph of a porous Y_2O_3 plate prepared from powder treated with dilute nitric acid. The fine reticulated structure results from precipitation of $Y_2O_3 \cdot 6H_2O$ crystallites on particle surfaces. The material shown in Fig. IV-3 was fired in air at 1100°C. The structure can be altered substantially by firing at higher temperatures, as shown in Fig. 4 (1350°C). Both materials are nominally 50% porous.

The use of transient pore formers is also being considered as a means of producing monolithic separators. Transient pore formers are volatile solids which are intimately mixed with the ceramic powders prior to consolidation. In the course of high-temperature processing, the pore formers are driven off, leaving voids in the structure corresponding to the volumes which

*Materials Science Division, ANL.

†Molybdenum Corp. of America, Louriers, Colo.

‡Mearl MR, Mearl Corp., Roselle Park, N.J.; Egg Albumin, Fisher Scientific, Fair Lawn, N.J.

**Model OTTO-1A, Mearl Corp., Roselle Park, N.J.

Fig. IV-3. Yttria Powder Treated with *3M* Nitric Acid and Sintered at 1100°C (6000X)

Fig. IV-4. Yttria Powder Treated with *3M* Nitric Acid and Sintered at 1350°C (6000X)

they occupied. The textile fibers, used as the pore formers, were oriented parallel to the plate faces during die pressing. Figure IV-5 is a transverse fracture section through a plate having anisotropic porosity.

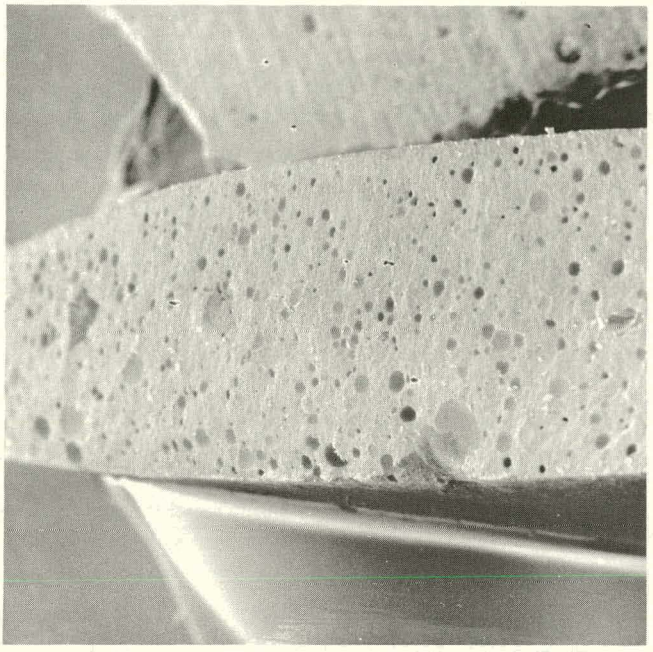

Fig. IV-5. Porous Yttria Plate Produced with the Aid of a Transient Pore Former (30X)

Effort is presently being directed toward refinement and characterization of porous structures produced by the techniques described. Characterization will include measurements of flexural strength, pore size and size distribution by mercury porosimetry, and resistance to gas flow (permeability). In-cell testing will be carried out in test cells of the type currently being used to evaluate flexible separators (ANL-76-35, p. 20).

4. Corrosion Studies
(J. A. Smaga)

Current collectors in the positive electrode are exposed to metal sulfides (FeS, FeS_2, Li_2S and Li_xFeS_y) and molten LiCl-KCl eutectic, a condition which results in rapid attack on most commonly used metals, *e.g.*, iron, nickel, copper and alloys of these elements. The corrosiveness of this environment is compounded by the fact that most metals react electrochemically with the electrolyte at potentials less than the normal charge cutoff potential of approximately 2.1 V for cells employing FeS_2 positive electrodes. For FeS positive electrodes, the conditions are less severe because of the reduced sulfur activity and the lower charge cutoff potential ($\sim$1.7 V). Because of the importance of developing current collectors, a number of metals have been subjected to corrosion tests in equal-volume mixtures of both FeS + LiCl-KCl and FeS_2 + LiCl-KCl for 500 to 1000 hr at 400, 450, and 500°C. The cumulative results for representative materials tested to date are summarized in Tables IV-2 and IV-3, which present both the corrosion rates and

Table IV-2. Compatibility Tests in FeS + LiCl-KCl

Material	Corrosion Rate,[a] μm/yr 400°C	450°C	500°C	Remarks
Molybdenum	1.8	3.1	10	Minor surface attack
Nickel	+13	+10	+49	Fe-Ni reaction layer
Niobium	+11	+26	+24	Fe-Nb reaction layer
Armco Iron	440	460	410	Severe intergranular attack
AISI 1008	620	-	-	Severe intergranular attack
Type 304 SS	3.8	3.6	9.0	Minor surface attack
Hastelloy B	1.8	2.5	+11	Complex reaction layer at 500°C
Hastelloy C	1.1	0.9	+18	Complex reaction layer at 500°C
Inconel 617	0.2	2.3	+18	Minor surface attack
Inconel 625	0.9	2.7	4.9	Minor surface attack
Inconel 706	-	4.6	-	Minor intergranular penetration
Inconel 718	-	5.0	-	Minor intergranular penetration
Incoloy 825	-	2.1	-	Minor surface attack

[a] Values preceded by a "+" sign indicate a net weight gain due to the presence of an adherent reactor layer.

Table IV-3. Compatibility Tests in FeS_2 + LiCl-KCl

Material	Corrosion Rate,[a] μm/yr 400°C	450°C	500°C	Remarks
Molybdenum	1.4	+1.0	+16	Weakly adherent MoS_2 layer
Nickel	2700	6600	6600	Very severe attack; Ni_3S_2, NiS
Niobium	720	2900	4500	Severe attack; intergranular penetration
Type 304 SS	3700	6000	6000	Very severe attack; FeS, $FeCr_2S_4$
Hastelloy B	83	490	4000	Intergranular penetration; NiS·FeS
Hastelloy C	160	680	3200	Minor intergranular penetration; NiS·FeS
Inconel 617	210	1000	1700	NiS, $NiCo_2S_4$, Cr_2S_3
Inconel 625	380	1000	1300	Probable NiS, Cr_2S_3
Inconel 706	-	3300	-	Severe attack; probable NiS, Cr_5S_6, $FeCr_2S_4$
Inconel 718	-	2400	-	Severe attack; NiS, Cr_5S_6, Ni_3S_2
Incoloy 825	-	3100	-	Severe attack; NiS·FeS, Ni_3S_2, $FeCr_2S_4$

[a] Values preceded by a "+" sign indicate a net weight grain due to the presence of an adherent reactor layer.

metallographic and microprobe observations for samples exposed to FeS + LiCl-KCl and FeS_2 + LiCl-KCl, respectively.

The results in Table IV-2 show that all of the materials, except Armco iron and AISI-1008, are suitable* for application in FeS cells. However, current collectors of low-carbon steel have been used in engineering-scale FeS cells with only minor corrosive attack. The results of tests in FeS_2 + LiCl-KCl (Table IV-3) indicate that, as expected, the corrosion rates for all of the metals were much higher in the FeS_2 environment than in the FeS environment. Molybdenum was the only material that showed an acceptably low reaction rate at all temperatures. The corrosion rate for Hastelloy B appears to be marginally acceptable at 400°C.

The brazed feedthrough requires corrosion-resistant, high-integrity brazed joints between the ceramic insulator and the metallic components, conducting rod, and cell housing. To facilitate the formation of this joint, Coors Porcelain Co. has developed several processes for metallizing the surfaces of Y_2O_3 ceramics. Compatibility tests were conducted on experimental samples of metallized samples to determine the suitability of these processes. The tests were conducted in equal-volume mixtures of LiAl and LiCl-KCl at a temperature of 450°C for 300 and 900 hr. The Y_2O_3 bodies had a flat ring geometry, and the flat surfaces were metallized by five different techniques. Multiple samples of each metallizing process were tested, and the weight losses within a group were quite consistent. On the basis of total sample weight, the weight losses were small, ranging from 0.02 to 0.12 wt %. The values listed in Table IV-4 represent the average weight loss per unit area of metallized surface for each group of samples. Because any weight loss contributed by the nonmetallized surfaces of the Y_2O_3 body could not be factored out, these values are maximum weight losses; the real losses could be even lower. Since the losses after 900 hr are only slightly greater than those after 300 hr, it is evident that the rate of weight loss decreases with time.

*Suitability based on corrosion rates that are 75 μm/yr or less.

Table IV-4. Compatibility and Bond Strength of Metallized Y_2O_3 Feedthrough Components

Metallizing Process Number	Average Weight Loss, mg/cm^2		Fracture Location
	300 hr	900 hr	
2	0.96	1.01[a]	Interface
4	0.83	0.94[a]	Interface
6A	0.36	0.44[a]	Interface
7B	0.20	-	Ceramic or metal layer
9B	-	0.21	Ceramic or metal layer

[a]Based on a single test sample.

The metallized bodies were returned to Coors for analysis of the post-test metallized bond strength. The samples were pulled in tension until fracture occurred. Fractures at the metal-to-ceramic interface indicate weak bond strengths; those through the ceramic body or metallized layer indicate a high-integrity bond. Table IV-4 also summarizes the location of fracture. On the basis of compatibility, bond strength, and metallizing composition, the "7B" metallizing process was selected as the optimum process. Brazed feedthrough assemblies which employ Y_2O_3 components metallized by this process will be supplied by Coors for further evaluation in half-cell tests.

5. Postoperative Examinations
(F. C. Mrazek, K. G. Carroll, J. E. Battles)

Postoperative examinations are conducted on test cells primarily to evaluate the performance of various construction materials and components, *e.g.*, feedthroughs, current collectors, electrode separators, and cell housings. These postoperative examinations provide important information, not only on the compatibility of cell components with the cell environment, but also on the performance and behavior of the lithium-aluminum and metal sulfide electrode materials. The examination procedures have been described previously (ANL-8109, p. 72).

a. Chemical Analyses of Five Prismatic Cells

Chemical analyses were performed on five vertical prismatic Li-Al/FeS_x cells during this report period. The samples for chemical analyses were obtained by cutting a vertical section of the positive electrode into nine equal sections. Sample number one was located at the top of the electrode. The odd numbered samples were submitted for total sulfur analysis; the even numbered samples were discarded. One negative electrode sample was also taken for each cell at a location corresponding to the number five position for the positive electrode.

Table IV-5 summarizes the results of the analyses for the five cells. These results show that the positive electrodes are reasonably homogeneous in sulfur and that no settling of the active materials is evident. Both positive and negative electrodes were analyzed for cross contamination by the opposing electrode and the results, such as aluminum in the positive electrode and sulfur in the negative electrode, indicated no significant cross migration of the active materials to the counter-electrode. The atomic ratio of chlorine to potassium was calculated from the results of the chemical analyses. For the LiCl-KCl eutectic composition, the atomic ratio is 2.38. Cells S-87 and IB/F1 show an abnormally high atomic ratio of 3.3. A shift of this magnitude in the electrolyte composition could result in an electrolyte that is partially solid at the cell operating temperature.

b. Formation of Li_2S in Electrode Separators

Recent examinations of FeS_2 cells have shown the presence of Li_2S in BN fabric and felt separators (ANL-76-98, p. 41). The Li_2S is crystalline and in most cases completely encapsulates one or more BN fibers. The crystal sizes usually range from 50 to 100 μm. The Li_2S has been observed in separator samples taken from the top, middle, and bottom of prismatic cells. Thus, the Li_2S is present as a more or less continuous zone in all areas of

Table IV-5. Results of Chemical Analyses on Positive and Negative Electrodes[a]

Cell Description	BB-1 Li-Al/FeS-Cu_2S 3493 hr 188 cycles	S-86 Li-Al/FeS_2-CoS_2 5250 hr 405 cycles	S-87 Li-Al/FeS_2-CoS_2 3460 hr 368 cycles	IB/F1 Li-Al/FeS-Cu_2S 334 hr 15 cycles	G-02-006 Li-Al/FeS_2-CoS_2 3456 hr 527 cycles
Negative Electrode					
Al	34.2	33.5	17.2	36.8	37.7
Cu	0.013	-	-	0.020	-
Co	-	0.003	0.023	-	0.024
S	<0.01	0.071	0.04	<0.02	0.06
Li	10.89	6.06	8.21	5.54	-
K	14.7	15.3	15.3	11.9	12.4
Cl	33.8	38.6	46.1	35.7	21.2
Atomic Ratio Cl/K	2.53	2.77	3.31	3.30	1.87
Positive Electrode					
Al	0.023	0.009	0.015	0.04	0.06
Cu	10.8	-	-	19.9	-
Co	-	1.16	1.62	-	1.14
K	9.43	13.4	13.4	11.0	14.4
Sulfur at Five Vertical Locations					
1 (top)	14.0	9.12	9.68	11.2	15.7
3	14.8	8.49	12.95	13.2	15.9
5 (middle)	15.8	8.18	11.04	15.0	16.9
7	14.9	8.18	9.98	14.0	14.2
9 (bottom)	14.4	8.81	10.70	12.8	16.7
Atomic Ratio S/Fe	0.93	1.78	1.61	0.88	1.41

[a]Analyses by N. L. Johnson, K. J. Jensen, and W. E. Streets of the Analytical Chemistry Laboratory.

the separators. Precipitates of iron are associated with the Li_2S crystals and are generally found at the interfaces of Li_2S and BN fibers and at the crystal surface. Ion and electron microprobe analyses* were used in the identification of the Li_2S and iron; aluminum was not detected by electron microprobe analysis. The identity of the Li_2S was confirmed by X-ray diffraction analysis.†

Table IV-6 lists the cells in which microscopic examinations have shown the presence of Li_2S in the separator. The first five entries are recent postoperative examinations, whereas the W-series are re-examinations of cells that were originally examined more than a year ago. Based on these results, it appears likely that Li_2S was formed in the separators of all FeS_2 cells that have been operated to date. Careful examination of FeS cells have shown no evidence of Li_2S in the separators. Attempts to correlate the presence of Li_2S in the separator with cell operating temperature, time, cobalt sulfide additive, and charge cut-off voltage have been unsuccessful. Additional tests are needed to determine whether a correlation does exist. Also, it is apparent that additional studies will be required to identify the mechanism involved in the formation of Li_2S. The microscopic and microprobe examinations suggest that the Li_2S was formed *in situ* with the precipitation of iron. The reactants are most likely species that are soluble in the electrolyte (*e.g.*, lithium-iron-sulfur compounds) at cell operating temperatures. The

*Performed by W. A. Shinn and D. V. Steidl, Chemical Engineering Division, ANL.

†Performed by B. S. Tani, Analytical Chemistry Laboratory, ANL.

Table IV-6. Li_2S in Separator

Cell No.	Temp., °C	Time, hr	Number of Cycles	Additive	Charge Cutoff Voltage, V
EP-2B4	450[a]	1900	140	cobalt sulfide	2.0
EP-2A4	425-435[a]	2736	409	cobalt sulfide	2.1
G-01-003	∿450	870	38	cobalt sulfide	cell overcharged
G-02-006	475	3456	522	cobalt sulfide	2.0-2.1
EC-1	450	∿120	25	cobalt sulfide	2.3
CCC-1	475	>7800	445	none	2.2-2.3
W-5	450	2137	111	none	
W-9	450	1500	76	none	-
W-12	450	194	10	cobalt sulfide	-

[a]Peak power test were conducted on these cells.

[b]Cell temperature was 512°C during start-up.

iron-sulfur-bearing species must be present only in FeS_2 cells (the only known such species are FeS_2 and Z-phase*) since this phenomenon does not occur in FeS cells. No evidence was found which would indicate that mechanical transport of discrete particles from the positive electrode was involved in this reaction.

c. Summary of Postoperative Examinations

Table IV-7 presents a summary of the postoperative cell examinations which were performed during this period, along with some conclusions as to the causes of failure.

B. Cell Chemistry
(M. F. Roche)

The objectives of the cell chemistry studies are (1) to investigate specific chemical and electrochemical problems that arise in the cell and battery development work, (2) to conduct studies that are expected to lead to improvements in the electrode and cell designs, and (3) to provide a basic understanding of the processes that occur within the cells.

1. Discharge Mechanism of FeS
(A. E. Martin, Z. Tomczuk)

The discharge of FeS electrodes in the presence of LiCl-KCl eutectic electrolyte leads to the formation of Li_2S and iron at full discharge, but

*Tentatively identified as $Li_4Fe_2S_5$ by A. E. Martin, Cell Chemistry Group.

Table IV-7. Summary of Cell Postoperative Examinations

Cell No.	Type of Cell	Hours of Operation	Number of Cycles	Reason for Termination	Postoperative Examinations
Al-4	Li_4Si/ FeS-Cu_2S	1600	6	Short circuit	Macro examination showed very little swelling in the negative electrode but considerable expansion of the positive electrodes. Severe Fe-Si reaction occurred with the structural components in the negative electrode. Stringers of metallic copper within the separator are believed to be the cause of the short circuit.
EP-2B4	Li-Al/ FeS_2-CoS_2	1900	140	Gradually declining performance	The electrolyte content in the entire cell was lower than normal. A short circuit was located in the bottom corner of the cell. Rupture of the retainer structure permitted the conductive negative electrode particles to extrude directly through the BN separator and eventually contact the positive electrode.
R-20	Li-Al/ FeS_2-CoS_2 (assembled uncharged)	317	9	Short circuit	A conductive path from positive electrode to bottom of cell was evident. Additional shorting resulted from the absence of BN separator cloth in a large region near the bottom of the cell.
EC-1	Li-Al/ FeS_2-CoS_2 (assembled uncharged)	110	25	Short circuit	Upward extrusion of positive electrode material into top of cell produced a short circuit at the fill tube. Removal of this short circuit revealed added shorting throughout the cell. The presence of a fairly continuous layer of Li_2S crystals within the BN felt separator was noted, and the phase was characterized by X-ray diffraction, electron probe, and ion probe micro-analysis. The phase forms *in situ* and surrounds the BN fibers, with accompanying precipitation of metallic iron.

(continued)

Table IV-7. (cont'd)

Cell No.	Type of Cell	Hours of Operation	Number of Cycles	Reason for Termination	Postoperative Examinations
G-02-001	Li-Al/ FeS-CuS[a]		1	Short circuit	Macro examinations of the cell section revealed that expanded mesh current collectors in the negative electrodes were tightly packed against each other and were located within the outer third of the electrode thickness. Severe corrosion of the mild steel current collectors in the positive electrode was evident, presumably as a result of accidental overcharging.
EP-2A4	Li-Al, Al/ FeS_2, CoS_2	2735	409	Declining performance	Metal components were not attacked appreciably and no short circuits had developed. A band of large Li_2S crystals (50 to 100 μm) found within the BN separator is believed to be the cause of declining performance.
EP-I-2-1	Li-Al/ FeS-Cu_2S	133	3	Short circuit	Both of these cells had Y_2O_3 felt separators with BN cloth at the edges. Multiple sectioning showed a short circuit caused by extrusion of positive electrode material through the junction of the Y_2O_3 felt and the BN cloth. The Y_2O_3 felt appeared to be performing well as a particle retainer in all other areas examined.
EP-I-1-A-2	Li-Al/ FeS-Cu_2S	474	23	Short circuit	

[a]The LiCl-KCl electrolyte in the negative electrode also contained $CaCl_2$.

the intermediate compounds, J phase ($LiK_6Fe_{24}S_{26}Cl$) and X phase (Li_2FeS_2), are also formed in electrodes that are only partially discharged. Photomicrographs of these phases, which are present in repeatedly cycled FeS electrodes, were presented in ANL-76-98, p. 47. Information on the kinetics of discharge of the intermediate phases has now been obtained by metallographic examination of FeS electrodes stopped at various stages of their first discharge. Lithium/FeS cells of 0.6-1.0 A-hr capacity were discharged at 400-430°C to 20, 40, 60, 80 and 100% of their capacity. Metallographic examination of the FeS electrodes showed that the surface of an FeS particle followed a different discharge path than its interior.

Photomicrographs that illustrate the reactions occurring at the surface and in the interior regions of the particles are shown in Fig. IV-6. The sequence of reactions is given below:

Stage I: Discharge of the FeS on the particle surface to J phase.

Stage II: Discharge of FeS in the particle interior to X phase.

Stage III: Discharge of X phase in the interior to Li_2S and iron.

Stage IV: Discharge of the surface layer of J phase to Li_2S and iron.

The differences in the exterior and interior mechanisms are attributed to a combination of (1) local enrichment of lithium ion as a result of J-phase formation on the particle surface (J-phase formation involves potassium from the LiCl-KCl), and (2) a high mobility of lithium ions through the J-phase surface layer. Because the X-phase interior discharges to Li_2S and iron prior to discharge of the J-phase exterior, it is possible that elimination of J phase would lead to better electrode performance.

Li-Al/FeS cells of about 1 A-hr capacity were also operated with LiCl-NaCl-KCl electrolytes to determine the effect of this change in electrolyte composition on J-phase formation. Addition of 9 mol % NaCl to the LiCl-KCl eutectic led to an improvement in the FeS discharge; two voltage plateaus, separated by about 30 mV and of nearly equal length, were observed. These plateaus, which are not observed in pure LiCl-KCl, appear to correspond to (1) discharge of both FeS and J phase to X phase, followed by (2) discharge of X phase to Li_2S and iron. Metallographic examination of an electrode stopped during its first discharge revealed that the surface layer of the FeS particles consisted of a mixture of J phase and X phase instead of J phase alone. Two other cells with 20 mol % NaCl in the electrolyte were also tested. This NaCl concentration led to poor cycling behavior because of the formation of NaCl crystals, and J phase was still found in the FeS particles. Apparently NaCl does not prevent J-phase formation but, at a reasonable concentration (9 mol %), it improves the kinetics of J-phase discharge.

In another Li/FeS cell of 0.4 A-hr capacity, the LiCl content of the LiCl-KCl eutectic (58 mol % LiCl) was increased to 70 mol % and the positive electrode was examined after 15% discharge. The amount of J phase found on the particle surfaces was much less than normal, which indicates that relatively minor decreases in potassium-ion concentration suppress J-phase formation. However, for good cell operation the electrolyte should be near the eutectic composition; saturation of the electrolyte with LiCl is not considered a practical approach.

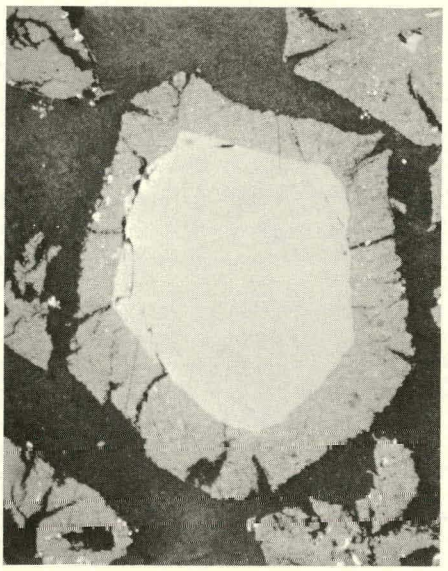

STAGE I. Inner Region-FeS; Outer Region--J ($LiK_6Fe_{24}S_{26}Cl$); Matrix--LiCl-KCl eutectic.

STAGE II. Inner Region--FeS; Intermediate Region--Li_2FeS_2, Fe; Outer Region--J.

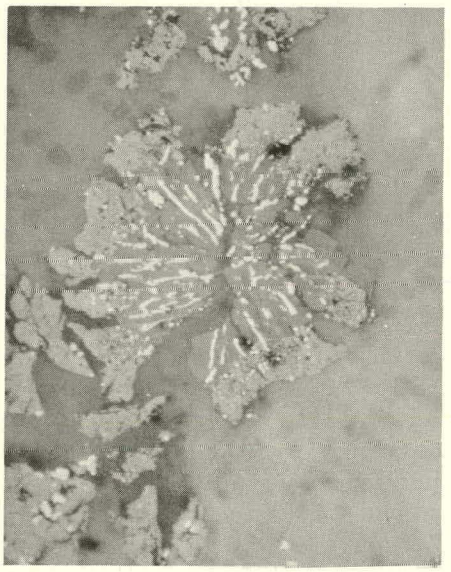

STAGE III. Inner Region--Li_2S,Fe; Outer Region--J.

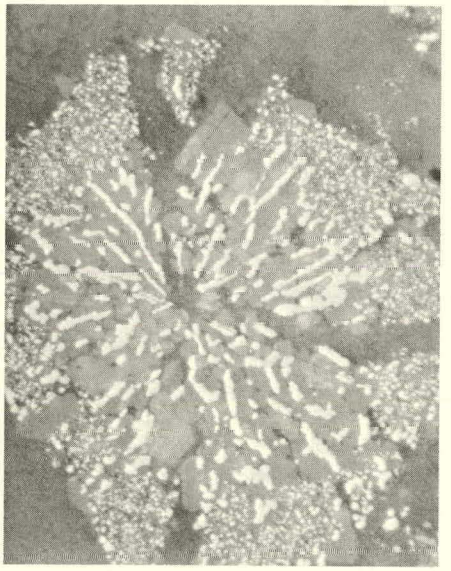

STAGE IV. Inner Region--Li_2S plus coarse Fe; Outer Region--Li_2S plus fine Fe.

Fig. IV-6. Changes Occurring in the FeS Particles During the First Discharge of Li/LiCl-KCl/FeS Cells. Original magnification 500X; as-polished. Photographically reduced by 35%.

2. Emf Measurements of LiAl/FeS_2 Cell
(C. Sy, Z. Tomczuk, M. F. Roche)

Preliminary results have been obtained for the emfs of the LiAl/FeS_2 couple as a function of temperature and state of discharge of the FeS_2 electrode. The measurements were made in a cell consisting of 1 A-hr of FeS_2 in a 5-cm^2 graphite housing, a 5 A-hr LiAl electrode in an iron housing, and LiCl-KCl electrolyte contained in an alumina crucible. The coulombic efficiency ranged from 97 to 99%, and >95% utilization of the FeS_2 was obtained when the cell was cycled at a temperature of 420°C and a current density of 12 mA/cm^2. The emf at 427°C (700 K) for the upper-plateau reaction (ANL-8057, p. 24)

$$4LiAl + 3FeS_2 \rightarrow 4Al + Li_4Fe_2S_5 + FeS$$

was 1.764 V and the temperature coefficient was 0.35 mV/°C. At the same temperature (700 K), the emf for the lower-plateau reaction

$$2LiAl + Li_2FeS_2 \rightarrow 2Al + 2Li_2S + Fe$$

was 1.327 V, with a temperature coefficient of -0.16 mV/°C. To provide a better thermodynamic description of the system, detailed emf measurements are being made in the transition region between the upper and lower voltage plateaus in which the positive electrode phases are transformed from $Li_4Fe_2S_5$ + FeS to Li_2FeS_2.

3. Positive Electrodes for Lithium Cells
(Z. Tomczuk, A. E. Martin, M. F. Roche)

A variety of transition-metal sulfides may be substituted for the iron-sulfide electrodes, FeS and FeS_2, in Li/metal sulfide cells, and some of the transition metal sulfides, such as Cu_2S and CoS_2, have been demonstrated to be useful additives for improving the performance of the iron sulfide electrodes. Because these alternatives to the iron sulfides are relatively expensive, they must produce a marked improvement in cell characteristics if they are to compete with the iron sulfides. In a continuing program to characterize the transition-metal sulfides, TiS_2 (and TiS_2 + FeS_2), V_2S_3, $CuCo_2S_5$ (prepared by the Electrochimica Corp.), and NiS_2 were tested in small Li/LiCl-KCl/metal sulfide cells. The metal sulfides were held in graphite-cup electrodes with porous graphite covers.

Earlier tests of TiS_2 (ANL-76-81, p. 53; ANL-76-98, p. 51) had been conducted at an electrode loading of only 90 mA-hr/cm^3. For the present test, the electrode loading was increased to 360 mA-hr/cm^3 by preparing a pressed pellet, 0.4 cm thick x 2.5 cm dia, of 4.2 g TiS_2 powder. In spite of the small volume fraction of electrolyte (estimated to be 0.15 from post-test examination), the electrode performance was as good as that of the less densely packed TiS_2 electrodes. Utilization of the 1 A-hr electrode was 97% at 100 mA/cm^2 discharge current density, and the cell voltage *vs.* fractional utilization curves were nearly identical for this cell and the earlier TiS_2 cells. This result suggests a very high mobility of lithium ions in the TiS_2. An electrode containing an equimolar mixture of FeS_2 (1.12 g) and TiS_2 (1.07 g) with a theoretical capacity of 1.25 A-hr was tested. The coulombic efficiency of the cell was poor (80%), and the combination of TiS_2 and FeS_2 did not appear to improve electrode performance.

The V_2S_3 and $CuCo_2S_5$ electrodes also had poor performance characteristics. The cell voltages were nearly the same as those of Li/FeS cells (approximately 1.7 V), but the electrode utilizations were less than 10% for V_2S_3 and ~30% for $CuCo_2S_5$ based on the total amount of sulfide present. The NiS_2 electrode gave more promising results. It exhibited discharge plateaus having emfs of 2.05, 1.86, and 1.64 V, in good agreement with thermodynamic calculations for the discharge of NiS_2 to NiS, Ni_3S_2 and finally, Ni. The electrode capacity was approximately 70% of the theoretical value of 3.65 A-hr/g Ni. A more detailed study of the NiS_2 electrode performance is planned.

4. Effect of Li_2S on Li-Al Electrodes
(S. K. Preto)

To study possible effects of Li_2S contamination on the operation of Li-Al electrodes, a negative-electrode-limited cell, SS-3, was constructed with a 15 A-hr FeS electrode and a 2 A-hr Li-Al electrode which contained 40 wt % Li-Al and 60 wt % Li_2S. Both electrodes had iron housings, Retimet current collectors, and areas of 15.6 cm^2. The cell was operated for more than 120 cycles with only minor coulombic inefficiencies, which were associated with accidental overcharge. The achieved negative electrode capacity was equal to the amount of Li-Al present, 2 A-hr, and the cell performance appeared to be largely unaffected by the presence of Li_2S in the negative electrode; the capacities to a 1-V discharge cutoff were 1.9 and 1.6 A-hr at current densities of 32 and 96 mA/cm^2, respectively. However, one unusual feature was the presence of three plateaus at potentials of 1.46, 1.38, and 1.32 V. The 1.46-V plateau, which represented about 60% of the charge capacity, is not seen in normal Li-Al/FeS cells. The compound responsible for this plateau has not been identified. The results of this test indicate that the presence of Li_2S may complicate the chemistry of the Li-Al electrode, but it does not appear to affect the capacity of the electrode.

5. Studies of Liquid Lithium Electrodes
(C. Sy, L. E. Ross, M. F. Roche)

Although the negative electrode material in present lithium/iron sulfide cells is a solid lithium-aluminum alloy, liquid lithium continues to be of interest because of its low equivalent weight and favorable electrochemical properties. The present studies have been aimed at maintaining preferential wetting of stainless steel substrates by the liquid lithium in the presence of molten-salt electrolyte.

An earlier experiment had shown that liquid lithium would wick down a corrugated sheet of iron to a depth of 9 cm in LiCl-KCl electrolyte (ANL-76-98, p. 46). However, attempts to obtain this type of behavior with a Type 304 stainless steel substrate of a similar geometry failed because the LiCl-KCl electrolyte preferentially wet the stainless steel. Additives that would promote retention of the liquid metal on the stainless steel were then sought in the belief that a solution to this problem would also aid in maintaining long-term stability of the liquid-metal electrode.

Alloys of lithium with Na, Ca, Cu, Al, Mg and Zn were heated in freshly machined Type 304 stainless steel cups under a helium atmosphere, and the temperature required to convert the liquid-metal meniscus from a convex (nonwetting) to a concave (wetting) shape was measured. This wetting

temperature was strongly dependent on stirring rate; stagnant alloys required temperatures in excess of 450°C. With rapid manual stirring with a stainless-steel rod, however, the results given in Table IV-8 were obtained. Only the smaller calcium addition appeared to be effective in lowering the wetting temperature.

Table IV-8. Wetting Temperatures for Lithium Alloys in Type 304 Stainless Steel Cups[a]

Alloy (wt %)	Wetting Temperature Range[b]
100 Li	193-224
80Li-20Na	268
90Li-10Ca	179-202
70Li-30Ca	214-224
30Li-70Ca	247
90Li-10Cu	197-227[c]
90Li-10Al	197-247[c]
90Li-10Mg	219-263[c]
80Li-20Zn	229-249

[a] Cups were 3 cm dia by 3 cm deep.

[b] At the lower temperature, the meniscus was concave over about 20% of the cup circumference (partial wetting). The meniscus was fully concave (complete wetting) at the higher temperature.

[c] Small, reddish colored buttons found floating on these alloys were identified as Li_2N with a trace of Li_2O.

When molten LiCl-KCl electrolyte was added to each of the above alloys in its Type 304 stainless steel cup, the wall of the cup was preferentially wet by the electrolyte. A variety of multiple-additive experiments were then conducted using binary and ternary combinations of Cu, Na, Ca, Al, Mg, Si, and Zn. These additions to the lithium were not particularly effective, but an addition of 1.2 mol % (10 wt %) copper to the lithium and 4.2 mol % LiF to the salt did produce the desired effect; the Li-Cu alloy rapidly filled the corrugations in a Type 304 stainless steel sheet when the sheet and alloy were placed in LiF-LiCl-KCl at about 400°C. Copper[3] and LiF* had been used previously to promote wetting of various substrates by alloys (Cu) or salts (LiF); this study showed the combination to be superior to either additive used alone in promoting lithium wetting of stainless steels. In addition, corrugated sheets and corrugated screens proved to be superior to Feltmetal, a porous metal substrate, because there was little spontaneous penetration

* Suggested by W. J. Walsh of the Chemical Engineering Division.

of liquid metal into the interior of the Feltmetal; filling of the V-shaped grooves (0.6 cm deep x 0.15 cm wide) by the alloy in the corrugated sheets and screens was spontaneous and rapid.

A Li-1.2 at. % Cu/LiF-LiCl-KCl/FeS cylindrical cell was constructed on the basis of the results of the wetting study. The cell had an 86 A-hr FeS electrode (4 cm in diameter x 10 cm high) on its central axis, and a 100 A-hr Li(Cu) electrode at its perimeter. The Li(Cu) alloy was held in vertically oriented grooves formed by pleating a screen (the "screen" was a layer of 325-mesh screen spot welded to each side of a 40-mesh screen). The cell has operated for more than 60 charge-discharge cycles with no evidence of short circuiting or dewetting. However, its capacity is only 25 A-hr, probably because of the large diameter of the FeS electrode; other cell designs are now being considered that should give better utilization.

C. Advanced Battery Research
(M. F. Roche)

The objective of this work is to develop new secondary cells that use inexpensive, abundant materials. The experimental work ranges from cyclic voltammetry studies and preliminary cell tests through the construction and operation of engineering-scale cells for the more promising systems. The studies at present are focused on the development of new cells with molten-salt electrolytes.

1. Emfs of Transition Metal Sulfide Cells
(M. F. Roche, Z. Tomczuk)

In connection with an experimental survey of metal sulfides, emfs were calculated for discharge of transition-metal sulfides, namely, sulfides of titanium through copper, by lithium, magnesium, and calcium at 700 K. Ternary compounds such as $Li_xM_yS_z$ were not considered; inclusion of Li_2S in the metal-sulfide phases often occurs in lithium cells, but as a rule leads only to a minor perturbation of the emfs. For sulfides that are stable at 700 K, free energies of formation from the elements and liquid sulfur were calculated using recent thermodynamic compilations.[4-6] The results are presented in Table IV-9.

Sulfur-rich compounds that decompose to sulfur and a lower sulfide were not included in Table IV-9, and some of the intermediate compounds listed, which were calculated to be unstable or only slightly stable toward decomposition into a mixture of their neighbors, were omitted from the emf calculations. Figure IV-7 gives the calculated emfs for the Li/metal sulfide cells as a function of state of charge. The emfs are 0.221 V higher for a negative electrode of calcium and 0.418 V lower for magnesium. A large area beneath the emf curve is equivalent to a high specific energy; only iron, cobalt, and nickel sulfides are capable of producing cells of very high specific energy.

The lower arrowhead along the right-hand boundary of each plot is the potential at which the metal produces a $10^{-3}M$ metal chloride solution (divalent except for CuCl), and the upper arrowhead is the overcharge potential of the highest sulfide to form $10^{-3}M$ metal chloride and sulfur. These potentials were calculated from molar potentials in LiCl-KCl given by Plambeck[7]

Table IV-9. Free Energies of Formation of Transition Metal Sulfides at 700 K (values in kcal/mol)

Ti	TiS	Ti_2S_3	TiS_2		
	-63.2	-171.7	-93.1		
V	VS	V_2S_3			
	-44.7	-119.3			
Cr	CrS	Cr_7S_8	Cr_5S_6	Cr_3S_4	Cr_2S_3
	-33.1	-248.2	-181.5	-112.4	-79.3
Mn	MnS				
	-53				
Fe	FeS	FeS_2			
	-24.5	-32.85			
Co	Co_9S_8	Co_3S_4	CoS_2		
	-187.9	-79.1	-30.8		
Ni	Ni_3S_2	$NiS_{0.84}$	NiS	NiS_2	
	-46.4	-17.6	-20.2	-26.5	
Cu	Cu_2S				
	-23.6				
Li	Li_2S				
	-100				
Mg	MgS				
	-80.7				
Ca	CaS				
	-110.2				

and the above sulfide data. Emfs for the metal chlorides in appropriate $CaCl_2$ and $MgCl_2$ salts, which are needed to determine overcharge emfs for calcium and magnesium cells, will be measured in future experiments.

2. Metal Oxide Electrodes
(S. K. Preto, M. F. Roche)

Metal oxide electrodes are being considered for use in secondary molten-salt cells (see ANL-76-98, p. 52). Studies of these electrodes consist of cyclic voltammetry measurements, thermodynamic calculations, and tests in laboratory-scale cells. Cells of two types are being considered:

1. $M'M''_x$/molten salt/$M'_yO \cdot Fe_2O_3$,Fe

2. $M'M''_x + M'_yO$/molten salt/$M'_yO \cdot Fe_2O_3$,Fe

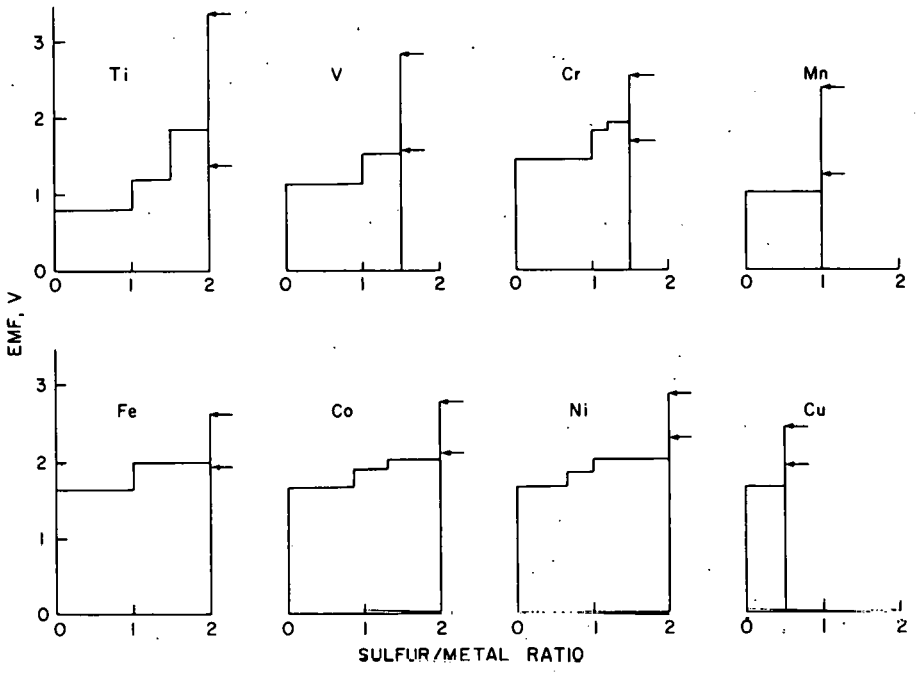

Fig. IV-7. Calculated Emfs for Li/Metal Sulfide Cells

The first type has a conventional alloy negative electrode such as Li-Al (M' = Li, M'' = Al, x = 1, y = 2) from which only M' discharges to form M' ions in the molten-salt phase. In the second type of cell, both M' and M'' are discharged, and, if the cell is to be reversible, the M'' ions must react with the M' oxide to form an M'' oxide and additional M' ions in the salt phase.

Cell emfs at 700 K were calculated from available thermodynamic data,[6,8,9] except for the calcium-aluminum data which were obtained from Ca-Al/FeS cell tests. Examples of possible overall cell reactions are listed in Table IV-10. A more detailed examination of the second and fourth reactions listed in the table showed that these cells would be impractical. Since lithium aluminate ($LiAlO_2$) can be reduced only at potentials very near that of lithium, liquid metal would form upon charging the 1.43-V cell. (Liquid metal was found in the negative electrode of a cell based on the 1.43-V reaction.) Calcium aluminate ($CaAl_2O_4$) is converted to $LiAlO_2$ in the presence of LiCl, according to thermodynamic calculations. Consequently, the fourth cell would

Table IV-10. Calculated Emf Data for Cells with Metal Oxide Positive Electrodes

(Type 1)	$3LiAl + LiFeO_2 \rightarrow 3Al + Fe + 2Li_2O$	1.15 V
(Type 2)	$3LiAl + 4LiFeO_2 \rightarrow 3LiAlO_2 + 4Fe + 2Li_2O$	1.43 V
(Type 1)	$3CaAl_2 + Ca_2Fe_2O_5 \rightarrow 6Al + 2Fe + 5CaO$	1.29 V
(Type 2)	$3CaAl_2 + 4Ca_2Fe_2O_5 \rightarrow 3CaAl_2O_4 + 8Fe + 8CaO$	1.36 V
(Type 1)	$3CaMg_2 + Ca_2Fe_2O_5 \rightarrow 6Mg + 2Fe + 5CaO$	1.54 V
(Type 2)	$CaMg_2 + Ca_2Fe_2O_5 \rightarrow 2MgO + 2Fe + 3CaO$	1.55 V

have the same problem as the second cell, namely, formation of liquid metal during charge (calcium cells are operated in LiCl-KCl-$CaCl_2$ electrolytes).

In a test of the first cell reaction listed in the table, lithium ferrate exhibited irreversibility; the charge polarization (450 mV at 16 mA/cm^2) was much greater than the discharge polarization (90 mV at 16 mA/cm^2). Therefore, lithium ferrate is considered to be an impractical electrode. Tests of the third reaction ($CaAl_2$ + $Ca_2Fe_2O_5$, 1.29 V) were conducted in a cell assembled in the uncharged state (Al/LiCl-KCl-$CaCl_2$/Fe + CaO). This cell operated reversibly for 55 cycles and had acceptable polarization characteristics. The positive electrode, which contained 5.6 g CaO and a large excess of iron, had a capacity of 3 A-hr. Thus, calcium ferrate appears to be a practical positive electrode material. Cells are being constructed to test the 1.54-V and 1.55-V $CaMg_2$ cell reactions, which employ the calcium ferrate positive electrode.

3. Calcium/FeS Cells
(L. E. Ross, A. E. Martin)

Negative-electrode compounds tested in earlier Ca/FeS cells were $CaAl_2$, $CaMg_2$, and Ca_2Si (ANL-76-36, p. 55 and ANL-76-81, p. 51). Ternary calcium intermetallics are now being evaluated. A ternary Ca-Mg-Si electrode was tested for 53 cycles at 460°C in an uncharged cell, Mg_2Si/(Fe+CaS). The electrolyte was (in mol %): LiF, 5.6; LiCl, 43.8; KCl, 11; $CaCl_2$, 39.6. The negative and positive electrodes contained 4.7 g Mg_2Si and 10 A-hr (Fe + CaS), respectively. The cell capacity corresponded to approximately 1 A-hr/g Mg_2Si, and its polarization characteristics were nearly a factor of two better than those observed in tests of the binary calcium compounds. The best $CaMg_2$ cell, for example, had a polarization equivalent to 4 Ω-cm^2 at 500°C in 2-min load tests (ANL-76-81, p. 52); the Ca-Mg-Si electrode polarization in a similar test was only 2.5 Ω-cm^2. Tests of $Ca_6Cu_3Al_7$ in a charged cell and of Al_2Cu in an uncharged calcium cell are now being conducted. These electrodes have relatively low charge-discharge capacities (0.3 A-hr/g Al-Cu), and their polarization characteristics are similar to those of Ca-Al electrodes.

A comparison of two of the important characteristics of the negative electrode compounds, namely, polarization behavior and compatibility with iron current collectors is given in Table IV-11; the compounds are listed in order of decreasing overall performance.

Table IV-11. Characteristics of Calcium Negative Electrodes

Compounds	Polarization Characteristics	Corrosiveness Toward Fe Current Collectors
Ca-Mg-Si	excellent	none
$CaMg_2$	good	none
$CaAl_2$	fair	mild
Ca-Al-Cu	fair	-
Ca_2Si	fair	strong

4. Engineering Studies

(D. R. Vissers, J. D. Arntzen, and K. E. Anderson)

Engineering studies of $CaAl_2/FeS$ and Ca_2Si/FeS cells have been reported previously (ANL-76-35, p. 56, and ANL-76-81, p. 54). Cell CA-7, an engineering-scale test of the $CaMg_2/FeS$ system, had a 60 A-hr negative electrode and a 90 A-hr positive electrode. The electrolyte composition in mol % was LiF, 5.60; LiCl, 43.74; KCl, 10.99; $CaCl_2$, 39.67. Operation of this cell was terminated after 53 cycles (1500 hr). The ampere-hour efficiency was high through 45 cycles but declined rapidly when the temperature was raised from 482 to 495°C in an attempt to improve the cell resistance. (The resistance was about 50 mΩ, which suggested poor wetting of the BN cloth separator by the electrolyte.) A postoperative examination indicated that liquid metal had formed in the negative electrode.

Engineering evaluations of the $Ca-(Mg_2Si)/FeS$ cell began with an uncharged cell, CA-8, which had a negative electrode containing 60 g Mg_2Si (about 60 A-hr) and an (Fe + CaS) positive electrode of 70 A-hr theoretical capacity. The electrolyte composition (in mol %) was: LiCl, 54.88; KCl, 38.14; $CaCl_2$, 6.98. The cell was operated for 20 cycles at 500°C when the test was terminated because of a short circuit. (Leakage of material through a 1-cm-dia hole in the positive-electrode retainer screen probably caused the short circuit.) The cell resistance was quite high (70 mΩ) which suggested poor wetting of the BN cloth separator by the electrolyte, as in Cell CA-7. Cell CA-8, prior to development of the short circuit, performed better than the cells that were tested earlier. Voltage-*vs.*-capacity curves are given in Fig. IV-8. The electrodes in Cell CA-8 were very thick (1.2 cm); the performance is expected to improve with thinner (0.6 cm) electrodes, which are now being fabricated for testing in a 100 A-hr prismatic cell.

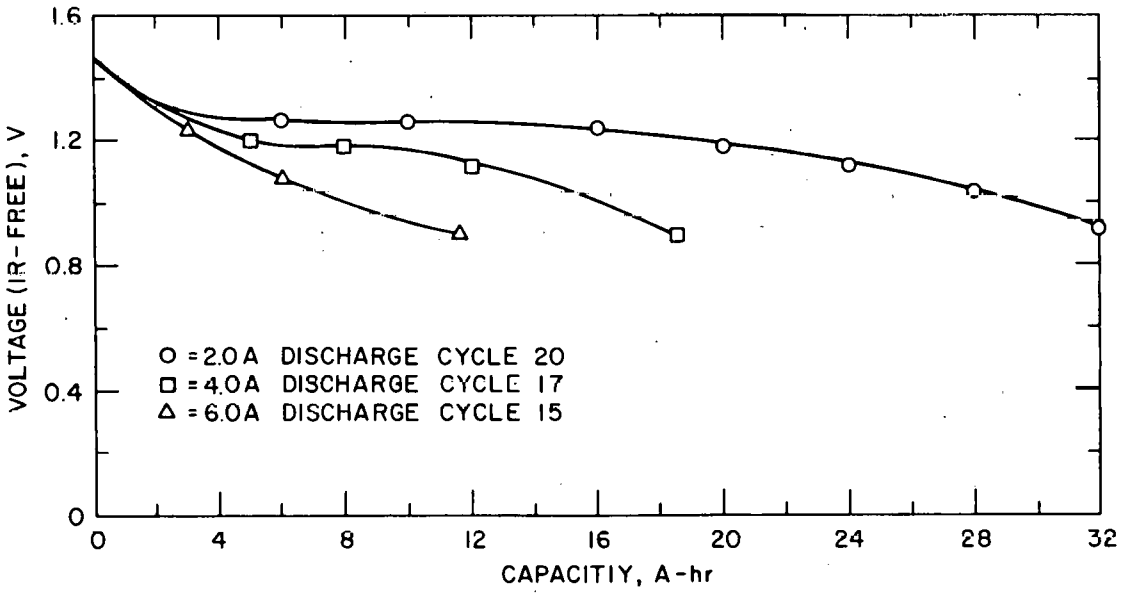

Fig. IV-8. Typical Voltage-*vs.*-Capacity Data for Cell CA-8

V. Li-Si/FeS CELL AND BATTERY DEVELOPMENT--ATOMICS INTERNATIONAL

A number of small compact bicells with electrodes 5 cm^2 in area were tested in this period with FeS electrodes and Li_4Si electrodes. All were built in the initially discharged state and all used brazed nickel positive electrode structures. Four types of separator materials were used. These included BN cloth (plasma-sprayed with $MgAl_2O_4$); rigid, porous AlN and Si_3N_4 plates; and a separator made by packing AlN powder in a cavity between adjacent electrodes. The last has yielded the most promising results, combining highly active positive material utilization (78%), low specific resistance (1.6 Ω-cm^2), and good coulombic and energy ($\sim$85%) efficiencies. Except for a lower active material utilization (52%), good results were also obtained with the porous Si_3N_4 separator. Cells with the powder separator and the porous Si_3N_4 remain on test. The superior overall results are attributed to the high porosity and low tortuosity of both types of separators.

Research on rigid, porous ceramic separators has been directed to maximizing the pore size of Si_3N_4 (β) and AlN plates to the degree permitted by strength requirements. A conductivity cell has been built to permit resistance measurements of these separators in molten-salt electrolyte. The results will be correlated with mercury porosimeter measurements. Preparations are being made for the fabrication of these separators in sizes up to 23 cm x 23 cm.

A 1.0 kW-hr multi-electrode demonstration cell placed in operation in early August completed 232 cycles in 3,430 hr of operation. The cell performance was excellent for 150 cycles, and an energy density of 79 W-hr/kg was achieved at the 11-hr rate. Thereafter, the coulombic efficiency declined steeply from its earlier value of 99%.

An instrumented 1.0 kW-hr cell is presently under construction for thermal characterization of large cells. Temperature excursions within the cell will be measured at a number of locations in the cell under various operating conditions. The large volume of data will be stored and processed by an automatic data acquisition system (DAS) which will also control the cell. The system will be checked out using the 1.0 kW-hr demonstration cell described above.

REFERENCES

1. E. J. Cairns, *et al.*, *Lithium/Selenium Battery for Implantation*, ANL-MDAP-70, pp. 50-52 (1970).

2. W. L. Towle, *et al.*, *Cost Estimate for the Commercial Manufacture of Lithium/Iron Sulfide Cells for Load-Leveling*, ANL-76-12 (1976).

3. L. R. McCoy, U. S. Patent No. 3,881,951 (May 6, 1975).

4. K. C. Mills, *Thermodynamic Data for Inorganic Sulphides, Selenides and Tellurides*, Butterworths and Co., Ltd., London (1974).

5. R. Hultgren, *et al.*, *Selected Values of the Thermodynamic Properties of the Elements*, American Society of Metals, Metals Park, Ohio (1973).

6. D. R. Stull and H. Prophet, *JANAF Thermochemical Tables*, 2nd Ed., NSRDS-NBS-37, U. S. National Bureau of Standards (1971).

7. J. P. Plambeck, J. Chem. Eng. Data *12*, 77 (1967).

8. I. Barin and O. Knacke, *Thermochemical Properties of Inorganic Substances*, Springer-Verlag, Berlin (1973).

9. N. P. Yao, L. A. Heredy and R. C. Saunders, J. Electrochem. Soc. *118*, 1039 (1970).

APPENDIX A.

SUMMARY OF LARGE-SCALE CELL TESTS

APPENDIX A. Summary of Large-Scale Cell Tests

Cell No.	Type of Cell	Operating Characteristics: Capacity, A-hr: Theor.	Operating Characteristics: Capacity, A-hr: Max.[a] at Indicated Rates	Operating Characteristics: Rates, hr: Disch.	Operating Characteristics: Rates, hr: Charge	Initial Eff.,[b] %: A-hr	Initial Eff.,[b] %: W-hr	Life Characteristics: Hours[c]	Life Characteristics: Cycles[c]	Life Characteristics: % Decline in: Capacity[d]	Life Characteristics: % Decline in: A-hr Eff.	Remarks
2A5	Li-Al/ FeS_2-CoS_2	69	55.6	5.6	5.6	99+	83	3050	310	29	8.7	Eagle-Picher thin electrodes. Max. specific energy, 65.8 W-hr/kg (5.6-hr rate); 41.6 W-hr/kg (4.1-hr rate) at 200 cycles. Terminated.
2B5	Li-Al/ FeS_2-CoS_2	149	114.7	8.8	8.8	99+	80	2175	127	27	33	Eagle-Picher thick electrodes. Charge cutoff 2.1 V. Capacity 71 W-hr/kg at 2000 hr. Terminated.
2B6	Li-Al/ FeS_2-CoS_2	149	117 68	11.6 4.5	11.6 4.5	99+	84	>936	>37	1	None	Eagle-Picher thick electrodes, used in evaluation of cell heating and cooling.
2B7	Li-Al/ FeS_2-CoS_2	149	124 91	9.5 4.0	9.5 7.0	99+	78	>1900	>350	12	None	Eagle-Picher thick electrodes. Operating on 7-day electric vehicle cycling schedule.
2B8	Li-Al/ FeS_2-CoS_2	149	118 117	11.8 9.0	11.8 9.0	99	82	>2400	>164	33	None	Start-up and operation with cell blanketed in Kaowool insulation, exposed to air.
I-1-A-1	Li-Al/ FeS-CuS_2	149	110	11	11	99+	84	>432	>18	~12	None	Eagle-Picher thick electrodes. Test of Y_2O_3 separator. Operated between 1.55 and 1.1 V cutoffs.
R-13	Li-Al/ FeS-Cu_2S	60	34	5	5	78	64	3408	695	40	10	Assembled uncharged; 20 mol % Cu_2S in FeS; 10 wt % $CaCl_2$ in LiCl-KCl eutectic. Terminated.
R-15	Li-Al/ FeS_2-CoS	168	109	5	7	98	57	2230	155	20	30	Assembled uncharged; FeS_2-CoS in honeycomb structure, pressed Al wire negative. Terminated.
R-17	Li-Si/ FeS-Cu S	120	61	6	13	63	47	553	43	60	62	Assembled uncharged; with LiSi as the starting material in honeycomb structure. Terminated.
R-18	Li-Al/FeS	120	65	5	7	97	80	1750	132	24	15	Assembled uncharged; FeS, no additive. Woven Al plaques with Cu coated strands in negative electrodes. Terminated.
R-19	Li-Si/ FeS-Cu_2S	120	81	16	16	95	80	938	45	55	77	Assembled charged; FeS-Cu_2S positive; Li_4Si powder in honeycomb structure as negative. Terminated.
R-20	Li-Al FeS_2-CoS_2	120	64	6	9	76	75	250	10	4	25	Assembled uncharged; negative electrode pressed Al wire. Terminated.
R-23	Li-Al $FeS_2 + CoS_2$	103	64	3	10	96	75	>678	>39	None	None	Upper-plateau cell assembled uncharged. Negative electrode, pressed Al wire; positive electrode, hot pressed.
R-24	Li-Al/ $FeS_2 + CoS_2$	112	100	5	14	93	65	>420	>17	None	None	Upper-plateau cell assembled uncharged. Negative electrode, pressed Al wire, partially charged; positive electrode, hot-pressed.

[a] Based on at least five cycles.

[b] Based on at least 10 cycles at the 5-hr rate.

[c] The "greater than" symbols denote continuing operation.

[d] Percent decline from maximum capacity at the 5-hr rate, except where noted.

APPENDIX A. (Cont'd)

Cell No.	Type of Cell	Operating Characteristics: Capacity, A-hr: Theor.	Operating Characteristics: Capacity, A-hr: Max.[a] at Indicated Rates	Operating Characteristics: Rates, hr: Disch.	Operating Characteristics: Rates, hr: Charge	Initial Eff.,[b] %: A-hr	Initial Eff.,[b] %: W-hr	Life Characteristics: Hours[c]	Life Characteristics: Cycles[c]	Life Characteristics: % Decline in: Capacity[d]	Life Characteristics: % Decline in: A-hr Eff.	Remarks
KK-4	Li-Al/ FeS_2-CoS_2	90	87	5	5	100	79	5000	350	49	1	Assembled charged; carbon-bonded FeS_2-CoS_2 and hot-pressed Li-Al; cell resistance 5.8 mΩ.
KK-5	Li-Al/ FeS-$CuFeS_2$	120	93	5	10	99	85	>5600	>320	5	1	Assembled uncharged; carbon-bonded Li_2S + Fe + Cu and Al wire plaque + Li-Al hot-pressed electrodes. Resistance has increased to 4.8 mΩ.
KK-6	Li-Al/ FeS_2-CoS_2	150	94	5	10	100	72	>4200	>280	15	1	Assembled uncharged; carbon-bonded Li_2S + Fe + CoS_2 and 32 at. % Li-Al solid plate electrodes.
I-3-A-1	Li-Al/ FeS-Cu_2S	150	125	12	12	99	81	>650	>30	20	1	An Eagle-Picher thick electrode cell which contained 10 wt % NaCl in the electrolyte.
CB-1	Li-Al/ $CuFeS_2$	147	67	5.2	5.5	98	67	>7800	>562	6	5	Charged, carbon-bonded $CuFeS_2$ electrode; hot-pressed Li-Al negative electrode. Open cell in sealed furnace well. Performance very stable.
SS-1	Li-Al/ FeS-Cu_2S	650	450	11	11	100	85	>2000	>92	7	1	Assembled charged; carbon-bonded FeS-Cu_2S and Li-Al in Fe Retimet; designed for utility application; 25 x 35 cm electrodes.
FM-1	Li-Al-In/ FeS-Cu_2S	70	46	6	6	97	82	>2460	>210	7	4	Charged, thin Eagle-Picher FeS-Cu_2S positive electrode; Li-Al-4 wt % In negative electrode. Performance relatively stable at 5-hr rate; cell resistance 7.3 mΩ.
FM-2	Li-Al-Ca/ FeS-Cu_2S	70	55	7	7	99	85	1775	126	24	24	Charged, thin Eagle-Picher FeS-Cu_2S positive electrode; Li-Al-8 wt % Ca negative electrode. Steadily declining A-hr efficiency. Cell terminated.
FM-3	Li-Al-Sn/ FeS-Cu_2S	70	48	6	6	99	84	>145	>6	None	None	Charged, thin Eagle-Picher FeS-Cu_2S positive electrode. Li-Al-8 wt % Sn negative electrode. Undergoing break-in cycling.
TO-3	Li-Al/ FeS_2-CoS	116	104	14	24	87	77	230	6	None	None	Uncharged, hot-pressed Li_2S + CoS + Fe; solid Li-Al negative plaque. In-house made separator. Cell developed short, terminated.
EC-1	Li-Al/ FeS_2-CoS	120	114	5	10	99	82	462	24	50	50	Assembled uncharged, positive electrode: hot-pressed. Negative electrode: Li-Al cast plaque.

[a] Based on at least five cycles.

[b] Based on at least 10 cycles at the 5-hr rate.

[c] The "greater than" symbols denote continuing operation.

[d] Percent decline from maximum capacity at the 5-hr rate, except where noted.

THIS PAGE

WAS INTENTIONALLY

LEFT BLANK

APPENDIX B.

SUMMARY OF BATTERY TESTS

APPENDIX B. Summary of Battery Tests

Battery Number	Battery Description	Operating Characteristics: Rate, hr: Disch.	Charge	Equalization	Performance at Indicated Rates: Max. Capacity, A-hr	Max. Energy, W-hr	Initial Eff., %: A-hr	W-hr	Life Characteristics: Hours[a]	Cycles[a]	% Decline from Max. at 5-hr Rate: A-hr	A-hr Eff.	W-hr	W-hr Eff.	Remarks
B7-S	2 Eagle-Picher Li-Al/FeS-Cu_2S thick cells in series. Theo. capacity, 149 A-hr. Total cell wt, 4.0 kg	23.4	23.4	4	117	289	98	80	>4152	>225	9	None	14	2	Total life of 1B4 is 5337 hr, 289 cycles; life of 1B6 is 4695 hr, 262 cycles. Now being operated with equalization after every cycle.
		10.0	8.5	4	100	246	99	80							
		5.1	6.2	4	77	176	99	74							
		2.8	4.1	4	57	124	99	72							
		1.4	3.5	4	35	78	99	70							
B8-S	2 Eagle-Picher Li-Al/FeS_2-CoS_2 thin cells in series. Theo. capacity, 69 A-hr. Total cell wt, 2.6 kg	9.9	10.0	0	50	140	98	78	2256	379	24	None	39	17	Total life of each cell (2A3 and 2A4) is 2736 hr, 409 cycles. Testing voluntarily terminated.
		5.0	4.5	0	50	135	99	78							
		2.2	6.2	0	44	103	99	66							
		1.2	4.9	0	24	47	98	53							
B9-S	2 Eagle-Picher Li-Al/FeS-Cu_2S thin cells in series. Theo. capacity, 69 A-hr. Total cell wt, 2.7 kg	10.6	10.0	0	53	154	98	85	>744	>66	10	None	13	None	Cells 1A7 and 1A8 now being operated with bulk charge only.
		7.0	7.0	0	53	134	99	86							
		5.1	5.0	0	51	127	99	83							
		3.2	4.9	0	49	115	99	78							

[a]The "greater than" symbols denote continuing operation.

APPENDIX C.

STATISTICAL DATA ON THE CELL AND BATTERY TESTS

Table C-1 shows the status of twenty-one experimental and industrial cells that were operated during October-December 1976. As can be seen from this table, some of these cells have been terminated during this period; others are still in operation. Figure C-1 depicts the number of cycles achieved by these FeS and FeS_2 cells. A detailed description of cell design and operating conditions can be found in Appendixes A and B. The cycle lifetime data of Fig. C-2 were derived from the data in Fig. C-1.

Table C-1. Status of FeS and FeS_2 Cells

Cause of Cell Termination	FeS Cells		FeS_2 Cells		Cell Total	
	No.	%	No.	%	No.	%
Separator Cut	--	--	2	18.2	2	9.5
Extrusion of Mat'l	--	--	2	18.2	2	9.5
Metal Sulfide in Sep.	1	10	--	--	1	4.8
Metal in Sep.	--	--	1	9.1	1	4.8
Quality Control	--	--	1	9.1	1	4.8
Voluntarily Term.	--	--	2	18.2	2	9.5
Unknown[a]	4	40	--	--	4	19.0
Operation Continuing	5	50	3	27.2	8	38.1

[a]Most of these cells did not undergo postoperative examination.

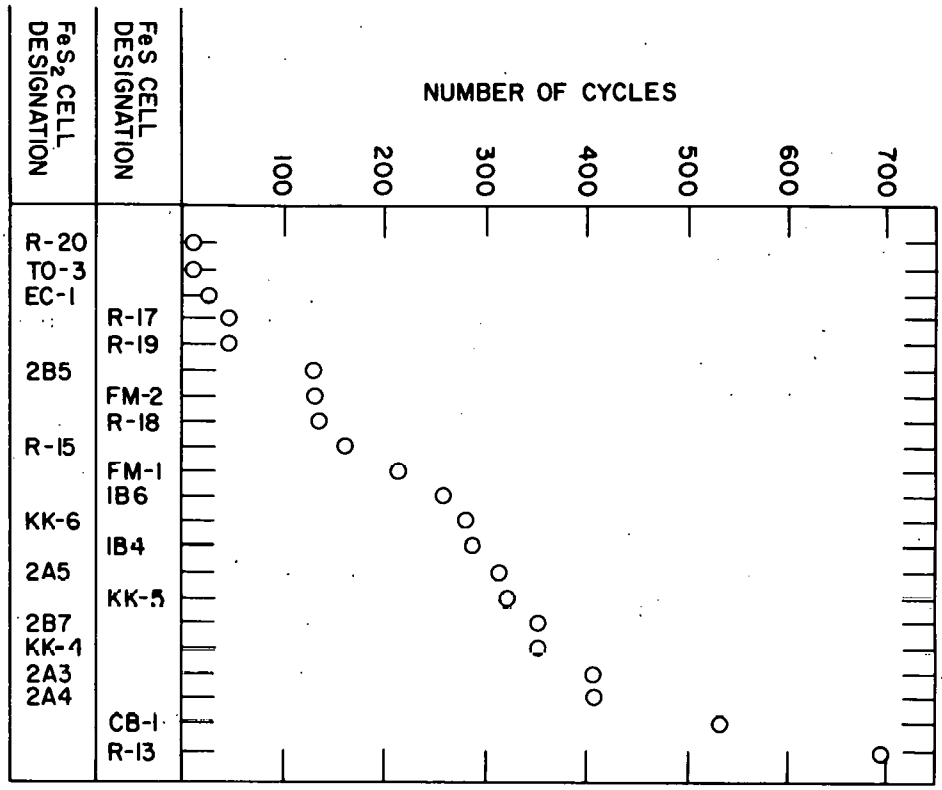

Fig. C-1. Number of Cycles Achieved by FeS and FeS_2 Cells

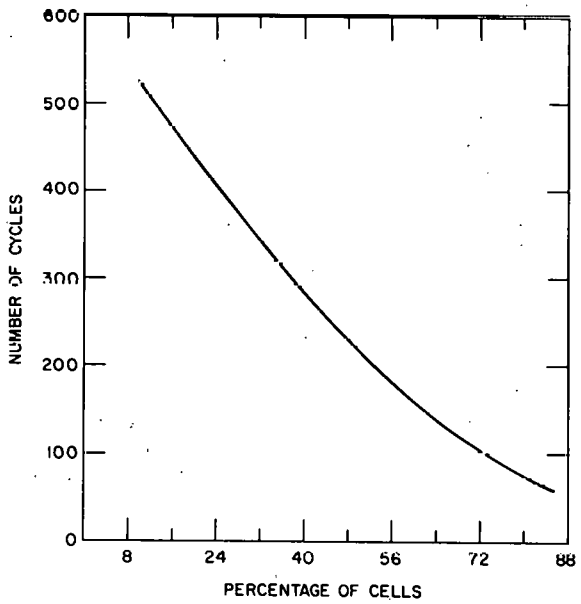

Fig. C-2. Cycle Lifetime Data of FeS and FeS_2 Cells

Distribution for ANL-77-17

Internal:

M. V. Nevitt
R. V. Laney
P. R. Fields
S. A. Davis
B. R. T. Frost
G. T. Garvey
D. C. Price
K. E. Anderson
J. D. Arntzen
J. Barghusen
L. Bartholme
J. E. Battles
E. C. Berrill
W. Borger
C. A. Boquist
L. Burris
F. A. Cafasso
A. A. Chilenskas
K. Choi
P. Cunningham
D. Day
W. DeLuca
J. Dorsey
R. Dunne
J. G. Eberhart
R. Elliott
W. R. Frost
E. C. Gay
J. Harmon
F. Hornstra
A. A. Jonke
R. W. Kessie
G. M. Kesser
V. M. Kolba
W. Kremsner
M. L. Kyle
W. W. Lark
S. Lawroski
R. F. Malecha
A. E. Martin
F. J. Martino
C. A. Melendres
A. Melton
W. E. Miller
F. Mrazek
K. M. Myles
T. Olszanski
P. A. Nelson (100)
E. G. Pewitt
E. R. Proud
S. Preto
G. Redding
M. F. Roche
L. E. Ross
W. W. Schertz
J. L. Settle
H. Shimotake
J. A. Smaga
R. K. Steunenberg
B. Swaroop
C. A. Swoboda
W. D. Tuohig
Z. Tomczuk
R. Varma
D. R. Vissers
S. Vogler
W. J. Walsh
D. S. Webster
I. O. Winsch
S. E. Wood
N. P. Yao
P. Eshman
J. E. A. Graae
J. L. Hamilton
J. Mathers
G. J. Bernstein
P. A. Eident
T. D. Kaun
J. E. Kincinas
K. Kinoshita
Z. Nagy
K. A. Reed
M. A. Slawecki
A. B. Krisciunas
ANL Contract Copy
ANL Libraries (5)
TIS Files (6)

External:

ERDA-TIC, for distribution per UC-94c (182)
Chief, Chicago Patent Group
V. Hummel, ERDA-CH
President, Argonne Universities Association
Chemical Engineering Division Review Committee:
- R. C. Axtmann, Princeton Univ.
- R. E. Balzhiser, Electric Power Research Institute
- J. T. Banchero, Univ. Notre Dame
- D. L. Douglas, Gould Inc.
- P. W. Gilles, Univ. Kansas
- R. I. Newman, Allied-General Nuclear Services
- G. M. Rosenblatt, Pennsylvania State Univ.

J. G. Ahlen, Illinois Legislative Council, Springfield
J. Ambrus, Naval Surface Weapons Center
J. N. Anand, Dow Chemical Co., Walnut Creek, Calif.
F. Anson, California Inst. Technology
P. Auh, Brookhaven National Laboratory
B. S. Baker, Energy Research Corp.

H. Balzan, Tennessee Valley Authority
K. F. Barber, Div. Transportation Energy Conservation, USERDA
H. J. Barger, Jr., U. S. Army MERDC, Fort Belvoir
T. R. Beck, Electrochemical Technology Corp., Seattle
J. A. Belding, Div. Conservation Research & Technology, USERDA
M. Benedict, Massachusetts Institute of Technology
D. N. Bennion, Univ. California, Los Angeles
J. Birk, Electric Power Research Inst.
J. Braunstein, Oak Ridge National Laboratory
M. Breiter, GE Research & Development Center
J. O. Brittain, Northwestern U.
R. Brodd, Parma Technical Center, Union Carbide Corp.
J. J. Brogan, Div. Transportation Energy Conservation, USERDA
E. Brooman, Battelle Memorial Institute, Columbus
D. M. Bush, Sandia Laboratories
E. Buzzelli, Westinghouse Electric Corp., Pittsburgh
E. J. Cairns, General Motors Research Lab., Warren, Mich.
E. Carr, Eagle-Picher Industries, Joplin
P. Carr, Energy Development Associates, Madison Heights, Mich.
Chloride Systems (U. S. A.) Inc., North Haven, Conn.
C. Christenson, Gould Inc.
M. Cohen, Univ. of Chicago
A. R. Cook, Int'l Lead Zinc Research Organization, Inc., New York City
D. R. Craig, Hooker Chemical Corp.
G. Cramer, Southern California Edison, Rosemead
F. M. Delnick, Sandia Labs.
W. Dippold, Div. Transportation Energy Conservation, USERDA
J. Dunning, General Motors Research Lab., Warren, Mich.
P. Eggers, Battelle Memorial Institute, Columbus
R. P. Epple, Div. Physical Research, USERDA
P. L. Fleischner, National Beryllia Corp.
J. H. B. George, Arthur D. Little, Inc.
J. Giner, Tyco Labs., Inc., Waltham, Mass.
C. Goddard, Div. Conservation Research and Technology, USERDA
G. Goodman, Globe-Union, Inc., Milwaukee
G. Gorten, Gorten and Associates, Sherman Oaks, Calif.
H. Grady, Foote Mineral Co., Exton, Pa.
S. Gratch, Birmingham, Mich.
D. Gregory, Institute of Gas Technology, Chicago
N. Gupta, Ford Motor Co.
N. Hackerman, Rice U.
G. Hagey, Div. of Energy Storage Systems, USERDA
R. Hamilton, Carborundum Co., Niagara Falls
W. Hassenzahl, Los Alamos Scientific Laboratory
L. A. Heredy, Atomics International
B. Higgins, Eagle-Picher Industries, Joplin
R. Hudson, Eagle-Picher Industries, Joplin
J. R. Huff, U. S. Army Mobility Equipment R&D Center, Fort Belvoir
R. A. Huggins, Stanford U.
R. A. Huse, Public Service Electric & Gas Co., Newark, N. J.
S. D. James, U. S. Naval Surface Weapons Center (3)
M. A. Jansen, Allegheny Power Service Corp. Greensburgh, Pa.
G. Janz, Rensselaer Polytechnic Inst.
H. Jensen, C&D Batteries, Plymouth Meeting, Pa.

F. Kalhammer, Electric Power Research Institute
K. Kinsman, Ford Motor Co.
R. Kirk, Div. Conservation Research & Technology, USERDA
K. W. Klunder, Div. of Energy Storage Systems, USERDA
J. Lagowski, Detroit Edison Utility Co.
J. J. Lander, Air Force Aero Propulsion Lab., Wright-Patterson AFB
A. Landgrebe, Div. of Energy Storage Systems, USERDA (6)
C. E. Larson, Bethesda, Md.
S. H. Law, Northeast Utilities, Hartford, Conn.
H. Leribaux, Texas A&M U.
D. Linden, U. S. Army Electronics Command, Fort Monmouth, N. J.
R. Llewellyn, Indiana State U.
P. S. Lykoudis, Purdue Univ.
G. Mamantov, U. Tennessee
J. McKeown, Office of Program Administration, USERDA
C. McMurty, Carborundum Co., Niagara Falls
R. McRae, ILC Technology, Sunnyvale, Calif.
D. Meighan, C. & D. Batteries, Plymouth Meeting, Pa.
R. Minck, Ford Motor Co.
F. Moore, Div. of Energy Storage Systems, USERDA
G. Murray, Detroit Edison Utility Co.
E. Nicholson, Esso Research & Engineering Corporate Res. Lab., Linden, N. J.
C. Pax, Div. Transportation Energy Conservation, USERDA
G. F. Pezdirtz, Div. of Energy Storage Systems, USERDA
R. Rightmire, Standard Oil of Ohio, Cleveland
R. Rizzo, Globe-Union Inc., Milwaukee
N. Rosenberg, Transportation Systems Center, Cambridge, Mass.
N. W. Rosenblatt, E. I. duPont de Nemours & Co., Wilmington
R. Rubischko, Gould Inc.
A. Salkind, ESB Inc., Yardley, Pa.
G. Scharbach, American Motors General Corp., Wayne, Mich.
T. Schneider, Public Service Electric & Gas Co., Newark, N. J.
R. I. Schoen, National Science Foundation
J. R. Schorr, Battelle Memorial Institute, Columbus
D. R. Schramm, Public Service Electric & Gas Co., Newark, N. J.
H. J. Schwartz, NASA Lewis Research Center
J. R. Selman, Illinois Institute of Technology
A. I. Snow, Atlantic Richfield Co., Harvey, Ill.
S. Srinivasan, Brookhaven National Laboratory
D. Stakem, Catalyst Research Corp., Baltimore
E. Steeve, Commonwealth Edison Co., Chicago
R. H. Strange II, National Science Foundation
R. L. Strombotne, U. S. Dept. Transportation, Washington
S. Sudar, Atomics International
R. H. Swoyer, Pennsylvania Power and Light Co., Allentown
F. Tepper, Catalyst Research Corp., Baltimore
L. Thaller, NASA Lewis Research Center
G. M. Thur, Div. Transportation Energy Conservation, USERDA
C. W. Tobias, U. California, Berkeley
L. Topper, National Science Foundation
J. Vanderryn, Office of Intern. R&D Programs, USERDA
J. V. Vinciguerra, Eagle-Picher Industries, Joplin
R. D. Walker, Jr., U. Florida
C. O. Wanvig, Jr., Globe Union, Inc., Milwaukee

S. A. Weiner, Ford Motor Co.
J. Werth, ESB Inc., Yardley, Pa.
C. Wienlein, Globe-Union Inc., Milwaukee
F. Will, General Electric R&D Center, Schenectady
J. Withrow, Chrysler Corp., Detroit
W. L. Wonell, U. of California, Berkeley
S. Wood, La Grange Park, Ill.
T. Wydeven, NASA Ames Research Center
O. Zimmerman, Portland General Electric Co., Portland, Ore.
M. Zlotnick, Div. Conservation Research and Technology, USERDA
Chloride Technical Limited, Manchester, England
E. Aiello, U. of Chicago
W. J. Argersinger, Jr., U. of Kansas
J. T. Banchero, U. of Notre Dame
K. J. Bell, Oklahoma State U.
R. Blanco, Oak Ridge Nat. Lab.
C. F. Bonilla, Columbia U.
W. Brandt, U. of Wisconsin-Milwaukee
A. E. Dukler, U. of Houston
W. J. Frea, Michigan Tech. U.
C. D. Harrington, Douglas United Nuclear, Inc.
J. E. Linehan, Marquette U.
Maine Univ., Prof. in charge of Chem. Engr. Lib.
Marquette U., Dept. of Chemistry
Michigan Tech. U., Library
G. Murphy, Iowa State U.
E. A. Peretti, U. of Notre Dame
G. W. Preckshot, Engr. U. of Missouri
H. Rosson, U. of Kansas
C. Sanathanan, U. of Illinois-Chicago Circle
A. Sesonske, Purdue U.
USERDA, Director, Div. of Safeguards and Security
B. W. Wilkinson, Michigan State U.
Comision Nacional de Energia Atomica, Library, Argentina
J. A. Sabato, Com. Nac. de Energia Atomica, Buenos Aires, Argentina
C. H. Cheng, Nat'l Tsing Hua Univ., China
National Radiological Protection Board, Library, Harwell, England
L. Kemmerich, Ges. fur Kernforschung, Karlsruhe, Germany
F. Weigel, Inst. fur Anorganische Chemie der U. Munich, Germany
N. Saratchandran, Bhabha Atomic Research Centre, Bombay, India
K. Fujimiya, U. of Tokyo, Japan
Japan Atomic Energy Research Inst., Tokai-mura, Japan
K. Matsuda, Inst. of Physical & Chemical Res., Yamato-machi, Japan
Sang-Soo Lee, Korea Advanced Institute of Science, Korea
Korean Atomic Energy Research Institute, Korea
Ragnar Nordberg, Sahlgren's Hospital, Goteborg, Sweden